Pertanika J. Sci. & Technol. 34 (2): 787 - 822 (2026)

PERTANIKA JOURNALS

SCIENCE & TECHNOLOGY

Journal homepage: http://www.pertanika.upm.edu.my/

Optimisation of Silver Nanoparticle Synthesis Using Aqueous Extract of *Passiflora foetida* L. via Response Surface Methodology

Silvia Handayani[1], Alyza A. Azmi[1], R. Rudiyanto[2], Wan Iryani Wan Ismail[1], Kustiariyah Tarman[3,6], Faridah Abas[4], Wan M. Khairul[1,5], and M. Maulidiani[1,5]*

[1]*Faculty of Science and Marine Environment, Universiti Malaysia Terengganu, 21030 Kuala Nerus, Terengganu, Malaysia*

[2]*Faculty of Food Science and Agrotechnology, Universiti Malaysia Terengganu, 21030 Kuala Nerus, Terengganu, Malaysia*

[3]*Department of Aquatic Products Technology, Faculty of Fisheries and Marine Science, IPB University, 16680 Bogor, West Java, Indonesia*

[4]*Department of Food Science, Faculty of Food Science and Technology, Universiti Putra Malaysia, 43400 UPM Serdang, Selangor, Malaysia*

[5]*Advanced Nano Materials (ANOMA) Research Group, Faculty of Science and Marine Environment, Universiti Malaysia Terengganu, 21030 Kuala Nerus, Terengganu, Malaysia*

[6]*Centre for Coastal and Marine Resources Studies, International Research Institute for Maritime,Ocean and Fisheries (i-MAR), IPB University, 16680 Bogor, West Java, Indonesia*

ABSTRACT

This study investigates the green synthesis of silver nanoparticles (PF-AgNPs) using the aqueous extract of the medicinal plant *Passiflora foetida* to enhance their biological activity. PF-AgNPs were characterised using UV-Vis spectroscopy, FTIR, XRD, SEM, and EDX analyses. The UV-Vis absorption peaks of PF-AgNPs were observed between 380 and 480 nm. Structural characterisation using FTIR and XRD confirmed that the functional groups of *P. foetida* metabolites acted as surface-capping agents, yielding crystallised AgNPs with a face-centred cubic (fcc) structure. SEM-EDX analysis further revealed that the synthesised PF-AgNPs were spherical and displayed a uniform distribution of silver at 66.39% under the optimised condition. The synthesis of PF-AgNPs was optimised using a Box–Behnken design via Response Surface Methodology (RSM), evaluating the effects of extract concentration (0.1%, 0.2%, and 0.3%), pH (4, 7, and 10), and temperature (30 °C, 50 °C, and 70 °C), with observations

ARTICLE INFO

Article history:
Received: 28 July 2025
Accepted: 26 February 2026
Published: 17 April 2026

DOI: https://doi.org/10.47836/pjst.34.2.09

E-mail addresses:
silvia.handayanni@gmail.com (Silvia Handayani)
alyza.azzura@umt.edu.my (Alyza A. Azmi)
rudiyanto@umt.edu.my (R. Rudiyanto)
waniryani@umt.edu.my (Wan Iryani Wan Ismail)
kustiaz@apps.ipb.ac.id (Kustiariyah Tarman)
faridah_abas@upm.edu.my (Faridah Abas)
wmkhairul@umt.edu.my (Wan M. Khairul)
maulidani@umt.edu.my (M. Maulidiani)
* Corresponding author

e-ISSN: 2231-8526

taken at 1 and 24 hours. UV-Vis intensity, NO scavenging activity, and DPPH scavenging activity were used as the response variables in RSM modelling. All models yielded p-values of less than 0.05, indicating that the factors significantly influenced PF-AgNP synthesis, with pH identified as the most effective parameter. PF-AgNPs exhibited DPPH and NO inhibitory activities of 35.64% and 38.7%, respectively, both of which were higher than those of the extract (17.16%). These findings highlight a sustainable and statistically guided approach for synthesising bio-functional AgNPs with promising potential for future biomedical applications.

Keywords: Antioxidant, green synthesis, *Passiflora foetida*, response surface methodology, silver nanoparticles

INTRODUCTION

Nanotechnology has been one of the fastest-growing fields and has rapidly become a powerful tool for tackling challenges in various areas, from medicine and pharmaceuticals to the food industry (De Silva et al., 2021; Naganthran et al., 2022). Among metallic nanoparticles, silver nanoparticles (AgNPs) have attracted particular attention due to their unique properties, including high conductivity and chemical stability. These features have made them useful in a wide range of applications, such as anti-inflammatory, antibacterial, and antioxidant activities (Alex et al., 2025; Barkat et al., 2017; Gherasim et al., 2020; Kaushal et al., 2023; Sytu & Camacho, 2018; Temur et al., 2024).

Green synthesis of AgNPs has gained popularity over traditional physical and chemical methods, largely because they are both eco-friendly and cost-effective (Alex et al., 2025; Pourmortazavi et al., 2015). Various biological resources have been used for AgNP production, including seaweed *Cladophora fascicularis* (Krishnamoorthi et al., 2022) and edible mushroom *Agaricus bisporus* (Rajasekar et al., 2019). The characteristics of the resulting nanoparticles can be influenced by several factors, including the type and concentration of biological reducers, precursor salt levels, reaction time, pH, and temperature (Crisan et al., 2021). Plant extracts are highly useful among various green methods due to their simple, fast, and economical synthesis with high reaction rates. Their phytochemicals, such as tannins, flavonoids, glycosides, alkaloids, polyphenols, enzymes and proteins act as reducing, stabilising and capping agents. They can also play the role of natural surfactants to promote NPs formation and stability (Abalkhil et al., 2017; Wang et al., 2021; Wasilewska et al., 2023).

Passiflora foetida, commonly known as passionflower, is a climbing plant of the genus *Passiflora* in the *Passifloraceae* family. The species has been widely distributed across tropical and subtropical regions due to its high adaptability and fast growth as a perennial tree. *P. foetida* has been reported to be a rich source of bioactive compounds. Thus, it might serve as a promising candidate for mediating the green synthesis of AgNPs. Its leaves have been used in folk medicine for the treatment of tuberculosis, stress, insomnia, helminthiasis, coughs, and colds (Díaz-Velasco et al., 2022; Patil et al., 2015).

Flavonoids, phenolics, glycosides, cyanogenic compounds, passifloricins, passifetilactone, α-pyrones, polypeptides, and alkaloids are the constituents of *P. foetida* associated with its biological activities (Nguyen et al., 2015; Song et al., 2018; Van Linh et al., 2022). However, this plant is frequently seen as a crop-harming weed. Previously, studies reported that the utilisation of plant extracts in the synthesis of AgNPs exhibited higher antioxidant activities compared to crude extracts (Gecer, 2025; Moges, 2022; Mazumder, 2025; Thapa et al., 2026). Although *P. foetida*-mediated AgNP synthesis has been reported, optimisation procedures for synthesis parameters such as pH, extract concentration, and temperature are lacking (Elangovan et al., 2022; Palanisamy et al., 2024). Traditional approaches for optimising reaction parameters vary only one factor at a time while keeping others constant. These methods are time-consuming and do not account for the simultaneous effects and interactions among multiple variables. In contrast, this study applied Response Surface Methodology (RSM) to systematically optimise *P. foetida*-mediated AgNPs synthesis. This approach provides a predictive model for reaction parameters, enabling maximised nanoparticle yield and improved physicochemical properties, representing the first optimisation model for this plant-based synthesis (Abu-Elghait et al., 2025; Ebrahimzadeh et al., 2020; Sati et al., 2025).

Therefore, this study focused on optimising the synthesis of AgNPs using *P. foetida* aqueous extract (PF-AgNPs) through RSM modelling, taking into account parameters such as pH, temperature, and extract concentration. Before PF-AgNPs synthesis, the chemical profile of *P. foetida* aqueous extract was analysed using ^{1}H NMR to identify the bioactive compounds that contribute to the reduction and stabilisation of silver ions. The UV-Vis, FTIR, XRD, and SEM analyses were carried out to confirm the formation and physicochemical characteristics of the obtained PF-AgNPs.

MATERIALS AND METHODS

Materials and Chemicals

The leaves of *P. foetida* were collected around the coastal areas of Universiti Malaysia Terengganu (UMT), the east coast of Peninsular Malaysia. The plant was identified by a Botanist, Dr Shamsul Khamis and the voucher specimen (ID068/ 2023) was deposited at the Herbarium Universiti Kebangsaan Malaysia (UKM), Malaysia. Leaf samples were cleaned with tap water and stored at -80°C before freeze-drying. A 20 g freeze-dried powder sample was extracted using distilled water at a ratio of 1:20 with ultrasonication at a temperature of 40°C. The water extract filtrate was then stored at -80°C for two days and subsequently freeze-dried to obtain a *P. foetida* aqueous extract.

All the chemicals and reagents used in this study were purchased from Sigma-Aldrich, Merck, Systerm, and Bendosen. The deuterium oxide (D_2O) containing 0.1% trimethylsilylpropanoic acid (TSP) sodium salt from Merck (Darmstadt, Germany)

was used for ^{1}H NMR analysis at 500 MHz (Varian Inc., California, USA). The chemicals used in AgNPs synthesis comprised silver nitrate ($AgNO_3$, Systerm), sodium hydroxide (1N NaOH, Bendosen), hydrochloric acid (1N HCl, Bendosen), and distilled water. In addition, chemicals including sodium nitroprusside (Solarbio), phosphate-buffered saline (PBS, Gibco), Griess reagent (Sigma-Aldrich), gallic acid (Sigma-Aldrich), quercetin (Aldrich), 2,2-diphenyl-1-picrylhydrazyl (DPPH, Sigma-Aldrich), methanol (Merck), and dimethyl sulfoxide (DMSO, Solarbio) were used for antioxidant assays. All the chemicals were of analytical grade.

Chemical Profiling of *P. foetida* Aqueous Extract by ^{1}H NMR Analysis

About 30 mg of *P. foetida* aqueous extract was added with 0.7 mL of D_2O containing 0.1% TSP, and the solution was sonicated at room temperature for 15 min (Maulidiani et al., 2018). After that, the solution was centrifuged at 13000 rpm for 5 min, and the supernatant was taken and transferred to an NMR tube. The ^{1}H NMR analysis was performed at a frequency of 500 MHz at room temperature 25 °C, with the parameters applied including number of scans of 64 and relaxation delay time of 2.0 s. The residual water signal at δ_H 4.70-4.90 ppm was suppressed through a pre-saturation method. Metabolite identification was conducted by comparing the characteristic signals of metabolites present in the ^{1}H NMR extract spectrum with the reference standards available via Chenomx Profiler software (Chenomx Inc., Edmonton, Canada) and literature data.

Design of Experiment via Response Surface Methodology (RSM) Modelling

Response Surface Methodology (RSM) was utilised to develop predictive models for optimising the experimental conditions of AgNPs synthesis. A Box-Behnken design (BBD) with three factors at three levels was employed to assess the effects of temperature, *P. foetida* extract concentration, and pH on the UV intensity of the resulting AgNPs (Table 1). A total of 14 experimental combinations of the independent variables. To model and analyse the relationship between the independent variables (temperature, *P. foetida* extract concentration, and pH) and the response variable (UV-Vis spectroscopy intensity), a second-order multiple linear regression model was used. This relationship is expressed by the following Equation 1:

$$Y = \beta_0 + \sum \beta_i x_i + \sum \beta_{ii} x_i^2 + \sum \beta_{ij} x_i x_j \quad [1]$$

where: In the regression model, Y represents the response variable (UV intensity), while x denotes the independent variables, with x_i and x_j representing the experimental

parameters, where i, j ranges from 1 to k. The model includes β as the regression coefficients, where β_0 is the intercept, β_i and β_{ii} represent the linear and quadratic coefficients, and β_{ij} indicates the interaction coefficients between variables. The term ϵ accounts for the random error. Model evaluation and statistical significance were assessed at a 95% confidence interval with $p < 0.05$.

Table 1
Selected parameters and their three-level

Factor	Units	Minimum	Maximum	Coded Low	Coded High	Mean
A: Temperature	ºC	30	70	-1	+1	50
B: Concentration of *P. foetida* extract	g/mL	0.1	0.3	-1	+1	0.2
C: pH		4	10	-1	+1	7

Synthesis of *P. foetida*-Silver Nanoparticles (PF-AgNPs)

$AgNO_3$ was used for the eco-friendly synthesis of AgNPs with *P. foetida* as the reducing and capping agents. The process involved mixing freeze-dried *P. foetida* extract solution with a 1 mM $AgNO_3$ solution in a 1:9 ratio within a 40 ml volume. The mixture was left at room temperature for 24 hours to observe at a range of 380-480 nm the reduction of Ag^+ ions to Ag^0 using a UV-Vis spectrophotometer (UV-1900i, Shimadzu Corp, UK) (Egodawaththa et al., 2022).

Characterisation of PF-AgNPs

The formation of PF-AgNPs was monitored using a UV–Vis spectrophotometer (UV-1800 Shimadzu 240V, Japan) within a wavelength range of 200 to 800 nm (Akash & Rehman, 2020). The functional groups were responsible for the reduction of Ag^+ to Ag^0, and the stabilisation of NPs was characterised using FT-IR spectroscopy (FT-IR INVENIO-S spectrometer, Bruker, Germany) with an attenuated total reflectance (ATR) accessory within the range of 4000–400 cm^{-1} at a resolution of 4 cm^{-1} with 16 scans. X-ray diffraction (XRD) was used to examine the crystallographic structure using a high-resolution Rigaku SmartLab, Japan, equipped with Cu-Kα radiation (λ = 1.5406 Å) at an operating voltage of 40 kV and current of 30 mA. Meanwhile, the diffraction was recorded at a range of 20–80°C (2θ) with a step size of 0.01° and a scan rate of 2°/min, and the crystallite size of the NPs was calculated using the Debye-Scherrer equation (Singh et al., 2018). The surface morphology of the synthesised AgNPs was characterised by scanning electron microscopy (SEM) performed using the VPSEM model LEO1455, and the elemental composition was determined by energy dispersive X-ray spectroscopy (EDX) analysis.

Before SEM imaging, AgNPs were coated with a thin layer of gold using a sputtering device and carried out at an accelerating voltage of 20 kV to obtain detailed surface morphology and elemental composition.

Antioxidant Assays

The antioxidant assays were performed using DPPH and nitric oxide (NO) scavenging methods Abdul-Hamid et al. (2019). Briefly, for the DPPH assay, 50 µL of the sample was mixed with 100 µL of DPPH reagent (5.9 mg/100 mL) in a 96-well plate and incubated for 30 minutes in the dark (Shata et al., 2025). Then, the absorbance was measured at λ_{max} = 515 nm. Quercetin was used as a positive control and methanol as a negative control in this experiment, and the percentage of inhibition was calculated using Equation 2. For the NO scavenging assay, 60 µL of the sample was mixed with 10 mM of PBS solution of sodium nitroprusside (SNP) in a 96-well plate and incubated for 150 minutes under light. Afterwards, 60 µL of Griess reagent (1% sulphanilamide, 0.1% NED, and 2.5% H_3PO_4) was added, and absorbance was measured at λ_{max} = 550 nm (Mohamad Ali et al., 2020; Sreejayan & Rao, 1997). The positive control was quercetin, while the negative control was DMSO.

$$\%\text{Inhibition} = \frac{(Ac - As)}{(As)} \text{ x } 100 \qquad [2]$$

Where A_c is the absorbance of the control or blank, A_s is the absorbance of the plant extract or AgNPs or standard.

Statistical Data Analysis

Analysis of variance (ANOVA) was used to determine the statistical significance of the regression model and its parameters. Model adequacy was assessed based on the *P*-value (< 0.05), F-value, R^2, adjusted R^2, and lack-of-fit statistics. All statistical analyses and 2D surface plot visualisations were conducted using the RSM package in R-Studio (https://www.r-project.org/), which enabled the identification of optimal synthesis conditions with a maximum of variable responses, indicating efficient AgNPs formation.

RESULTS AND DISCUSSION

Chemical Profile of *P. foetida* Aqueous Extract

In a green synthesis of NPs, it is hypothesised that the presence of the -OH group in primary and secondary plant metabolites is attributed to their capability to reduce silver ions to AgNPs.

In this study, the metabolite profile of *P. foetida* extract was analysed using ^{1}H NMR spectroscopy. Mainly, the aqueous extract of *P. foetida* consisted of aromatic (δ_H 6.0–8.5 ppm), glycoside (δ_H 3.1–3.9 ppm), and aliphatic (δ_H 0.7–2.5 ppm) compounds (Figure 1). Table 2 presents the identification of ^{1}H NMR characteristics of the metabolites in the *P. foetida* aqueous extract. Several aromatic compounds from the flavonoid class were identified, including vitexin derivatives at δ_H 8.01 (d, J= 8.5 Hz, H2' and H6'), 7.04 (d, J=8.5 Hz, H3' and H5'), and 6.69 (s, H3) as well as apigenin at δ_H 7.89 (d, J= 8.5 Hz, H2' and H6'), 6.84 (d, J= 8.5 Hz, H3' and H5') and 6.67 (s, H3). Amino acids such as phenylalanine, 4-hydroxyphenyllactic acid, glutamic acid, glutamine, alanine, valine, isoleucine, and leucine were also identified in the ^{1}H NMR spectrum. Further observation demonstrated that glycosidic compounds such as flavonoid glycosides were the major components of *P. foetida* aqueous extract. The chemical constituents of *P. foetida,* such as flavonoids, have been linked to its pharmacological effects, including antioxidant (Foudah et al., 2019; Ning et al., 2023), anti-inflammatory (Nguyen et al., 2015), and anticancer activities (Ponsuwan et al., 2024).

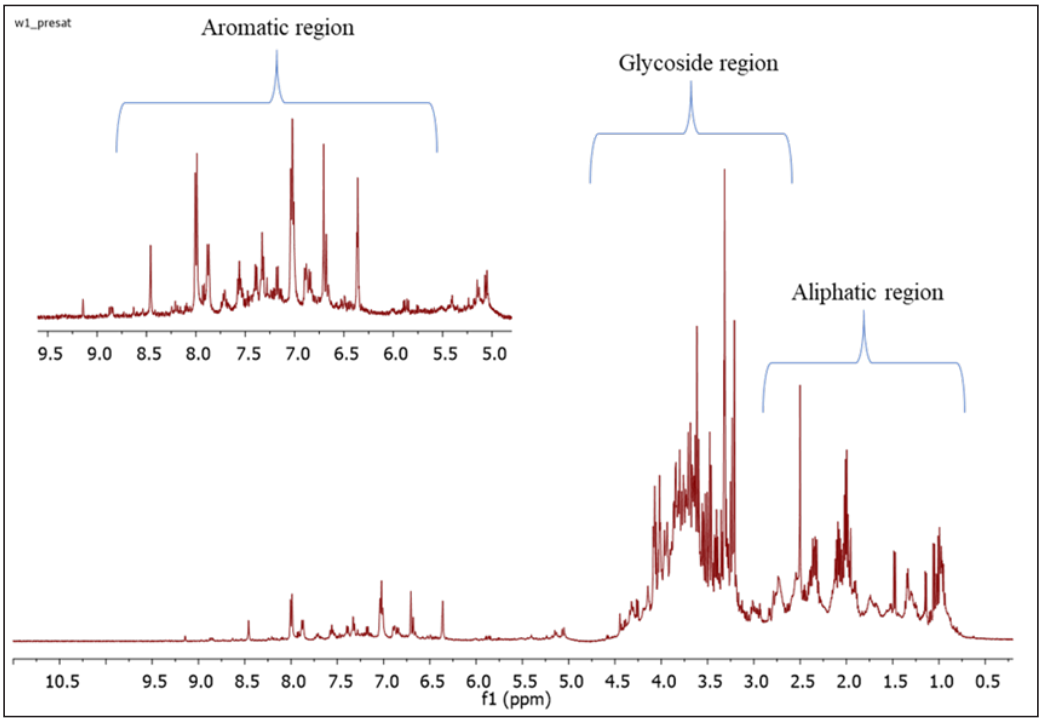

Figure 1. ^{1}H NMR spectrum of *P. foetida* aqueous extract in D_2O containing 0.1% TSP

Table 2
^{1}H NMR characteristics of the metabolites in P. foetida *aqueous extract*

HMDB ID	Compounds	Class	Chemical shift
HMDB0000687	Leucine	Amino acids	3.73 (m, ov.), 1.75–1.67 (m, ov.), 0.94 (t, J =4.75 Hz)
HMDB0250806	Valine		3.62 (d, J =4.45 Hz), 2.26 (m, ov.), 1.04 (d, J=7.05 Hz), 0.99 (d, J=7.00 Hz)
HMDB0000167	Threonine		4.25 (m, ov.), 3.60 (d, ov.), 1.33 (d, J=6.50 Hz)
HMDB0001310	Alanine		3.79 (q, ov.), 1.47 (d, J= 7.25 Hz)
HMDB0001080	4-aminobutyrate		3.01 (m, ov.), 2.29 (t, ov.), 1.90 (m, ov.)
HMDB0000162	Proline		4.12 (m, ov.), 3.41 (m, ov.), 3.33 (m, ov.), 2.34 (m, ov.), 2.06–1.98 (m, ov.)
HMDB0000020	4-hydroxy phenyllactic acid		7.16 (d, J= 8.50 Hz), 6.83 (d, J=8.55 Hz), 4.20 (m, ov.), 2.99 (m, ov.), 2.80 (m, ov.)
HMDB0000904	Citrulline		6.36 (br s), 3.75 (m, ov.), 3.15 (m, ov.), 1.84 (m, ov.), 1.59 (m, ov.)
HMDB0000172	Isoleucine		3.67 (d, ov.), 1.99 (m, ov.), 1.46 (m, ov.), 1.25 (m, ov.), 0.99 (d, J=7.00 Hz), 0.94 (t, J= 7.45 Hz)
HMDB0000182	Lysine		3.75 (t, ov.), 3.01 (t, J=8.15 Hz), 1.91 (m, ov.), 1.72 (m, ov.), 1.48 (m, ov.)
HMDB0000696	Methionine		3.85 (m, ov.), 2.63 (t, ov.), 2.19 (m, ov.), 2.13 (s)
HMDB0000159	Phenylalanine		7.42 (m, ov.), 7.37 (m, ov.), 7.31 (d, J=6.80 Hz), 3.99 (m, ov.), 3.28 (m, ov.), 3.12 (m, ov.)
HMDB0000191	Aspartate		3.89 (m, ov.), 2.79 (m, ov.), 2.67 (m, ov.)
HMDB0000929	Tryptophan		7.72 (d, J=7.70 Hz), 7.54 (d, J=7.65 Hz), 7.31 (s), 7.26 (m, ov.), 7.20 (m, ov.), 4.06 (m, ov.), 3.46 (dd, J=14.80 Hz, 4.9 Hz)
HMDB0000158	Tyrosine		7.19 (d, ov.), 6.87 (d, J=8.45 Hz), 3.93 (m, ov.), 3.20 (dd, ov.), 3.05 (m, ov.)
HMDB0000296	Uridine	Nucleosides	7.86 (d, J=8.55 Hz), 5.90 (m, ov.), 4.34 (m, ov.), 4.24 (t, ov.), 4.12 (m, ov.), 3.90 (m, ov.), 3.80 (m, ov.)

Table 2 (*continued*)

HMDB ID	Compounds	Class	Chemical shift
HMDB0304632	Glucose	Sugars	5.22 (d, J=3.65 Hz), 4.64 (d, J=8.10 Hz), 3.89(dd, ov.), 3.82 (m, ov.), 3.71 (m, ov.), 3.48 (m, ov.), 3.40 (m, ov.), 3.22 (m, ov.)
HMDB0000258	Sucrose		5.39 (d, J=3.45 Hz), 4.21 (d, ov.), 4.04 (t, J=8.80 Hz), 3.88 (m, ov.), 3.76 (t, 9.70 Hz) 3.66 (d, J=11.5 Hz), 3.56 (m, ov.)
HMDB0000660	Fructose		4.10 (m, ov.), 4.03 (dd, J=12.50 Hz, 1.20 Hz), 3.99 (m, ov.), 3.89–3.78 (m, ov.), 3.71–3.67 (m, ov.) 3.59–3.54 (m, ov.)
HMDB0000765	Mannitol		3.86 (m, ov.), 3.79 (m, ov.), 3.74 (m, ov.), 3.67 (m, ov.)
HMDB0000163	Maltose		5.39 (d, J=3.45 Hz), 5.22 (d, J=3.85 Hz), 4.65 (d, ov.), 3.97 (m, ov.), 3.97–3.58 (m, ov.), 3.42 (t, ov.), 3.28 (m, ov.)
HMDB0000646	Arabinose		5.29 (d, ov.), 5.23 (m, ov.), 4.51 (d, J=7.60 Hz), 4.11–3.64 (m, ov.), 3.51 (m, ov.)
HMDB0000098	Xylose		5.19 (d, ov.), 4.56 (d, J=7.85 Hz), 3.92 (m, ov.), 3.67– 3.62 (m, ov.), 3.51 (m, ov.), 3.42 (t, ov.), 3.30 (t, ov.), 3.22 (m, ov.)
HMDB0000975	Trehalose		5.18 (d, J=6.55 Hz), 3.86–3.76 (m, ov.), 3.46 (t, J=9.90 Hz)
HMDB0000956	Tartaric acid	Organic acids	4.34 (s)
HMDB0000254	Succinic acid		2.38 (s), 2.43 (s)
HMDB0005807	Gallic acid		7.02 (s)
HMDB0000691	Malonic acid		3.09 (s)
HMDB0000148	Glutamic acid		3.75 (m, ov.), 2.36–2.04 (m, ov.)
HMDB0000641	Glutamine		6.87 (s), 3.77 (t, ov.), 2.47–2.11 (m, ov.)
HMDB0000639	Mucic acid		4.25 (s), 3.95 (s)
HMDB0000625	Gluconic acid		4.13 (d, ov.), 4.03 (t, ov.), 3.84 (m, ov.), 3.77 (m, ov.), 3.66 (m, ov.)
HMDB0000097	Choline	Vitamins	4.06 (m, ov.), 3.51 (m, ov.), 3.19 (s)
HMDB0000244	Riboflavin		7.99 (s), 7.97 (s), 5.13 (m, ov.), 4.96–3.73 (m, ov.), 2.48 (s)

Table 2 (*continued*)

HMDB ID	Compounds	Class	Chemical shift
HMDB0128581	Hispidulin	Flavonoids	8.00 (d, J=8.75 Hz), 6.47 (s)
HMDB0301981	Isoorientin		6.71 (s)
HMDB0030614	Orientin		6.65 (s), 6.33 (s)
HMDB0005800	Luteolin		7.39 (d, J= 7.15 Hz), 6.85 (d, J= 8.35 Hz), 6.57 (s), 6.52 (d, J=3.45 Hz), 6.32 (d, J=3.85 Hz)
HMDB0030614	Vitexin		8.01 (d, J = 8.50 Hz), 7.04 (d, J = 8.50 Hz), 6.69 (s)
HMDB0002124	Apigenin		7.89 (d, J=8.50 Hz), 6.84 (d, J=8.50 Hz), 6.67 (s)
HMDB0253708	Isovitexin		6.67 (s)
HMDB0005801	Kaempferol		8.01 (d, J=9.00 Hz), 7.04 (d, J=9.00 Hz)

Note. Ov. is overlapped with other signals. Letters in parentheses refers to the signal multiplicities: s, singlet; d, doublet; t, triplet; dd, doublet of doublets; q, quartet; and m, multiplet

Optimisation of PF-AgNPs Synthesis using RSM Modelling

The optimisation experiments were conducted to synthesise the PF-AgNPs according to the BBD matrix, and evaluated the effects of temperature (X_1), extract concentration (X_2), and pH (X_3) on UV-Vis intensity, NO scavenging activity, and DPPH free radical activity (Table 3). The correlation matrix, as summarised in Figure 2a, indicated that pH exhibited the strongest positive correlation with UV-Vis intensity (r = 0.83), while temperature and concentration showed weaker correlations (0.28 and 0.16, respectively). This finding reinforces the hypothesis that pH plays a key role in the formation of AgNPs. Importantly, pH emerged as the most statistically significant individual factor ($P < 0.001$) (Seifipour et al., 2020), which highlighted the dominant influence of pH on UV absorbance intensity compared to other synthesis parameters. The synergistic effect between pH and temperature further suggests a cooperative influence on nanoparticle synthesis efficiency, underscoring the importance of optimising these conditions to enhance both structural and functional outcomes.

The regression model for UV-Vis intensity was statistically significant (F = 5.52; $P = 0.0052$), with a high coefficient of determination ($R^2 = 0.985$) on Figure 2b, a low root mean square error (RMSE = 0.097), and no significant lack of fit (P = 0.15), indicating good model adequacy. Among the three variables that were shown as a linear model,

Table 3
A Box-Behnken design under RSM for the synthesis of PF-AgNPs

Sample	Run	Factor 1	Factor 2	Factor 3	Respond 1	Respond 2	Respond 3
		Temp. ºC	Conc. (g/mL)	pH	Intensity (a.u)	NO %	DPPH %
A1B2C1	1	30	0.1	7	0.32	14.58	25.19
A2B1C1	2	30	0.2	4	0.26	10.83	27.00
A2B3C1	3	30	0.2	10	1.04	28.97	19.93
A3B2C1	4	30	0.3	7	0.62	22.21	14.29
A1B1C2	5	50	0.1	4	ND	10.94	20.35
A1B3C2	6	50	0.1	10	1.25	23.99	7.81
A2B2C2	7	50	0.2	7	0.74	22.21	15.02
A2B2C2	8	50	0.2	7	0.68	22.72	18.47
A3B1C2	9	50	0.3	4	1.77	35.15	19.60
A3B3C2	10	50	0.3	10	2.07	20.48	10.38
A1B2C3	11	70	0.1	7	0.72	27.18	19.04
A2B1C3	12	70	0.2	4	ND	21.18	28.44
A2B3C3	13	70	0.2	10	2.92	38.70	35.64
A3B2C3	14	70	0.3	7	0.94	18.23	23.28

Note. A= Concentration; B = pH; C = Temperature; ND = Not Detected; % = Inhibition (with the inhibition of *P. foetida* aqueous extract being 17.16%).

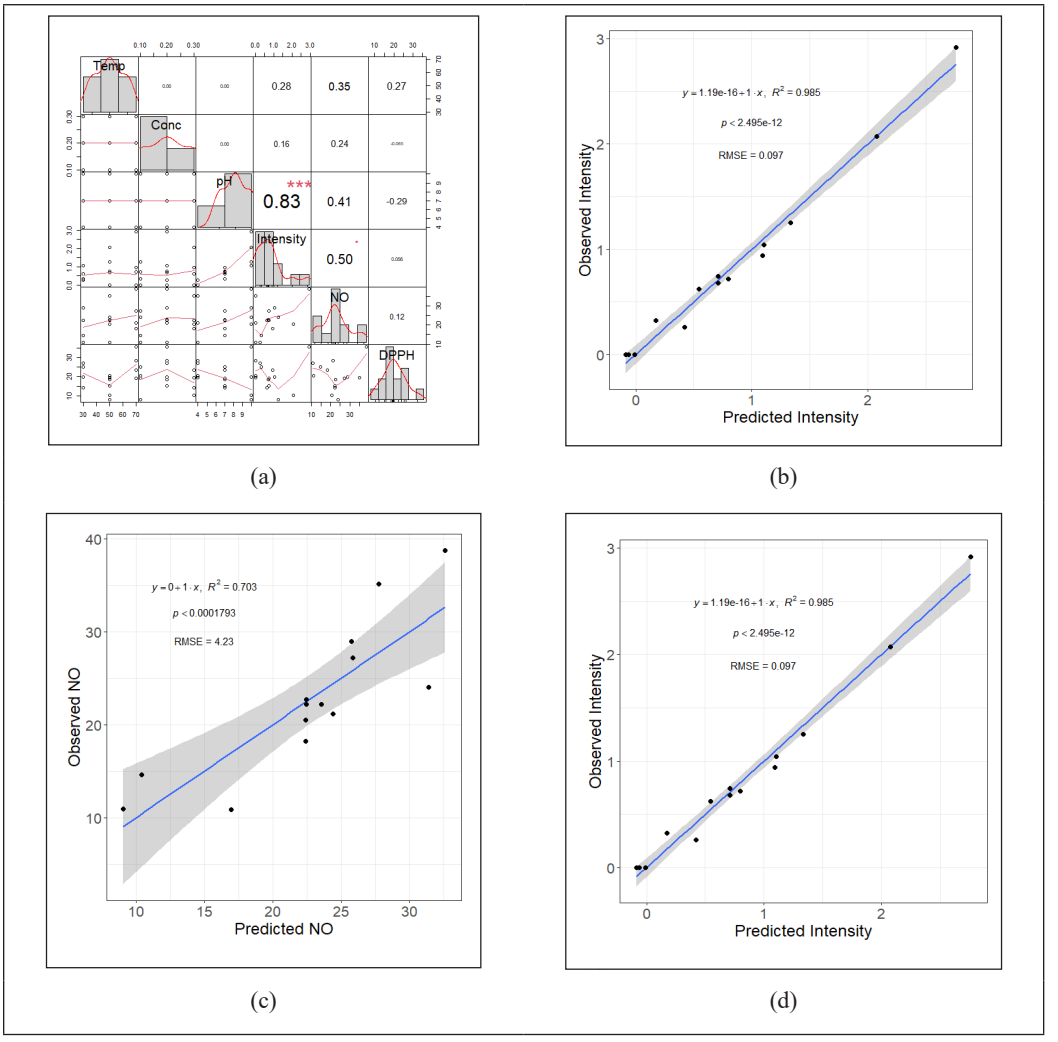

Figure 2. (a) Correlation between all factors with variable responses. Regression values; (b) intensity response; (c) NO scavenging response; and (d) DPPH scavenging response

pH (X_3) had the most significant effect ($P < 0.001$), followed by temperature (X_1; $P < 0.05$), while extract concentration was not statistically significant ($P = 0.059$). It is important to emphasise that the P values from this data set fall short of the strict < 0.0001 threshold (Patil et al., 2024). which suggests that the model lacks statistical significance. However, terms within the model that exhibit P values < 0.05 are still regarded as significant, indicating a greater probability (up to 5%) that the observed results occurred by chance (Desai et al., 2008; Ndikau et al., 2017). Further, the significant interaction was also observed between temperature and pH (X_1X_3; $P < 0.01$), showing the two-factor interaction. The maximum intensity (~2.95) at high temperature (~70°C), pH (~10), and higher concentration (~0.28%)

was suggested by the response surface plots (Figure 3a). However, at pH 4, NPs agglomeration was more evident, particularly at high temperatures, which may compromise product stability (Al-Gebory & Mengüç, 2018; Cativa et al., 2020).

The regression equation is graphically represented by two-dimensional response surface plots for NO scavenging activity that are statistically significant (F = 4.01; $P = 0.01598$) in Table 4, according to an R^2 of approximately 0.703 and an RMSE of 4.23 (Figure 2c). The model did not, however, appear to adequately capture the variability of the data, as indicated by a significant lack of fit ($P = 0.02899$). No individual variable or interaction term was statistically significant ($P > 0.05$). For the interaction factor BC (X_2X_3; $P < 0.155$), there is a trend toward interaction, although it cannot yet be statistically categorised as significant. The surface response plots under various pH conditions show slight curvature, indicating a tendency for a two-factor interaction between concentration and pH, although not significant plots (Figure 3b).

The model for DPPH scavenging activity was statistically significant (F = 4.73; $P = 0.0091$) in Table 4, with an R^2 of approximately 0.857 and RMSE of 2.68 (Figure 2d), as well as no significant lack of fit ($P = 0.30685$). The adequacy of the quadratic model was checked by ANOVA, and the temperature (X_1^2) was significant ($P = 0.0391$). The response surface plots in Figure 3c show a downward curve due to the DPPH activity decreasing in a range of moderate temperatures (~50–60°C), which marked the green area as dark, and the red to white area indicates higher values of DPPH activity.

Canonical path (Appendix) and response surface analyses (Figure 3a, 3b and 3c) showed that the stationary points for intensity, NO, and DPPH corresponded to saddle points, indicating the absence of true interior optima within the experimental design space. For all responses, predicted values decreased toward the centre of the canonical distance and increased toward the boundaries, confirming that optimisation is governed by boundary conditions rather than interior stationary points. Accordingly, particle swarm optimisation was applied to identify the maximum predicted responses within the experimental region. The optimal conditions for intensity were a temperature of 70 °C, a concentration of 0.30 g/mL, and pH 10, yielding a predicted value of 2.97 (a.u.). For NO, the maximum response (39.16 %) was predicted at 70 °C, 0.10 g/mL, and pH 10, while DPPH reached its optimum (31.96 %) at 70 °C, 0.242 g/mL, and pH 10. These results indicate that all three responses are strongly influenced by high temperature and alkaline pH, whereas the effect of concentration is variable, suggesting that careful adjustment of these factors can maximise the desired outcomes. The predicted optima provide a clear guide for experimental validation, which will further confirm the conditions for maximum response. These results were similar to earlier reports, thus confirming the effectiveness of RSM in determining the optimal conditions for the synthesis of plant-based AgNPs with desired physicochemical and biological properties (Aliero et al., 2024; Fernando & Zhou, 2019; Krupa et al., 2016).

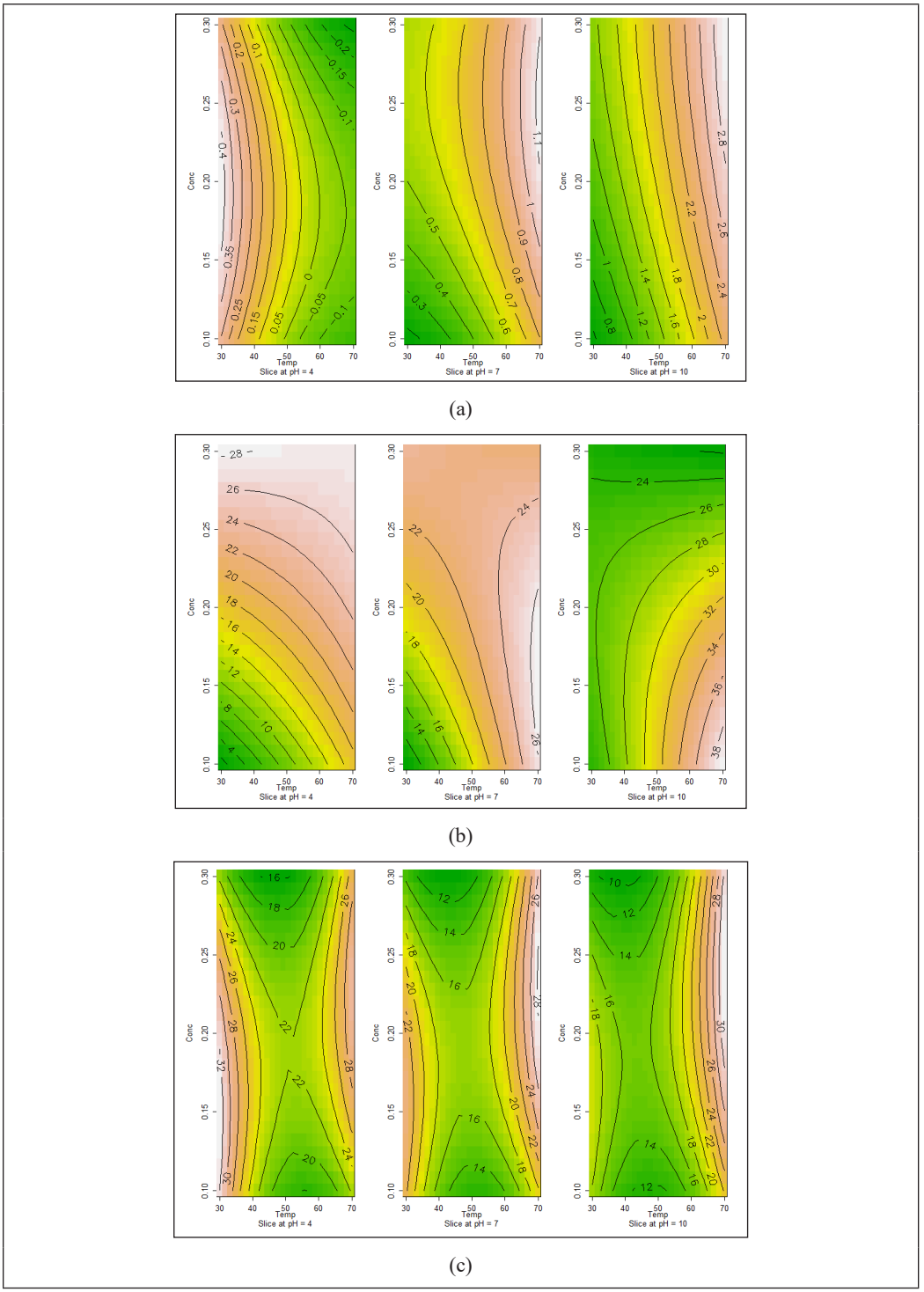

Figure 3. 2D response surface curves showing correlation: (a) intensity response; (b) NO scavenging response; and (c) DPPH scavenging response

Table 4
Optimisation studies of variable response using ANOVA

Source	Sum of Squares	Mean Squares	F-value	P-value	Remarks
Intensity responses					
Model	0.71	0.128623	5.52	0.005259	Significant
A-Temperature	0.2925	0.064311	4.5482	0.010432*	Significant
B-Concentration	0.1675	0.064311	2.6045	0.059763	
C-pH	0.8775	0.064311	13.6446	0.000167 **	Significant
AB	-0.02	0.09095	-0.2199	0.836715	
AC	0.535	0.09095	5.8824	0.004174	Significant
BC	0.205	0.09095	2.254	0.087259	
A^2	0.0825	0.101685	0.8113	0.462693	
B^2	-0.1425	0.101685	-1.4014	0.233717	
C^2	0.2625	0.101685	2.5815	0.06123	
Residuals	0.1324	0.03309			
Lack of fit	0.1306	0.04352	24.1759	0.148148	
Pure error	0.0018	0.0018			
NO Scavenging					
Model	22.465	5.6	4.0116	0.01598*	Significant
A-Temperature	3.5875	2.8	1.2812	0.26934	
B-Concentration	2.4225	2.8	0.8652	0.43575	
C-pH	4.255	2.8	1.5196	0.20323	
AB	-4.145	3.9598	-1.0468	0.35429	
AC	-0.155	3.9598	-0.0391	0.97065	
BC	-6.93	3.9598	-1.7501	0.155	
A^2	0.1825	4.4272	0.0412	0.96909	
B^2	-2.0975	4.4272	-0.4738	0.66036	
C^2	2.2725	4.4272	0.5133	0.63479	
Residuals	250.881	62.720			
Lack of fit	250.751	83.584	642.7049	0.02899	
Pure error	0.130	0.130			
DPPH Scavenging					
Model	16.7450	3.5432	4.726	0.009131	Significant
A-Temperature	2.4987	1.7716	1.4105	0.231226	
B-Concentration	-0.6050	1.7716	-0.3415	0.749913	
C-pH	-2.7037	1.7716	-1.5262	0.201669	
AB	3.7850	2.5054	1.5107	0.20538	
AC	3.5675	2.5054	1.4239	0.227574	
BC	0.8300	2.5054	0.3313	0.75706	
A^2	8.4612	2.8011	3.0206	0.039138*	Significant
B^2	-4.7562	2.8011	-1.6980	0.164746	
C^2	2.5463	2.8011	0.9090	0.414764	
Residuals	100.43	25.108			
Lack of fit	94.48	31.494	5.2920	0.30685	
Pure error	5.95	5.951			

UV-visible Spectroscopy Analysis

The formation of AgNPs can be observed by the colour change of the reaction mixture from yellowish to brownish-red, indicating the development and stabilisation of the NPs, as seen in Figure 4a. This also indicates that the phytochemicals of *P. foetida* were involved in the biosynthesis of AgNPs as a reducing agent. The distinctive surface plasmon resonance (SPR) band of the formed AgNPs have absorption bands of 380-480 nm (Egodawaththa et al., 2022). According to our observations, synthesis with a 24-h incubation time exhibited an absorption band for SPR compared to a 1-h incubation. Thus, for the RSM design experiments, synthesis with a 24-h incubation was chosen. For instance, the optimal condition A2B3C3 has SPR at 420 nm. Similar findings were reported for AgNPs synthesised from *Cicer arietinum* (Mouriya et al., 2023), *Sambucus ebulus* (Karan et al., 2024), *Diospyros malabarica* (Bharadwaj et al., 2021), *Lythrum salicaria* (Corciovă et al., 2022), and *Pyrus pashia* (Khanal et al., 2023).

The temperature effect has been evident in the increased synthesis rate of AgNPs formation with rising temperature. Previous studies indicate that higher temperature causes more thermal activity and a faster rate of crystal formation around the nucleus, which increases absorption (Liu et al., 2020; Xu et al., 2020). This improvement was marked by the growth in the size of NPs (Ebrahimzadeh et al., 2020). Figure 4b. illustrates the variation in the absorption spectrum of PF-AgNPs synthesised at temperatures of 30 and 70ºC, with a constant composition of extract concentration of 0.2% and pH 10. The temperature of 50ºC was not included in this variation as it adheres to the standard design of the BBD. At 0 hours, both samples (Figure 4b) exhibit the same colour with the starting SPR at 384 nm. After 24 hours at temperatures of 30ºC and 70ºC, the respective SPRs are 385 nm and 420 nm, exhibiting reddish-brown and brownish-red colours. The peak plasmon resonance shifts to longer wavelengths (redshift), and the intensity is greater, especially at the temperature condition of 70ºC. The resulting brownish-red colour indicated a significantly higher formation of AgNPs. These results are consistent with previous reports suggesting that an increase in temperature accelerates the reaction rate and enlarges the particle diameter (Liu et al., 2020). Optimisation studies confirm a temperature of around 70°C as ideal. An increase in extract concentration enhances the bioactive compounds involved in the reduction process.

Figure 4c illustrates the variation in the absorption spectrum of PF-AgNPs synthesised at extract concentrations of 0.1% and 0.3% (w/v), with constant pH and temperature compositions set at pH 10 and 50ºC. The concentration of 0.2% was not included in this variation as it adheres to the standard design of the BBD. At 0 hours, both exhibit the same SPR at 381 nm with higher intensity at the 0.3% concentration. After 24 hours, a shift in SPR occurs at extract concentrations of 0.1% and 0.3%, with respective SPRs of 415 nm and 406 nm, both exhibiting a brownish-red colour. The peak plasmon resonance shifts to longer

wavelengths (redshift), with a larger plasmon shift at the 0.1% concentration, indicating the formation of larger NPs compared to the 0.3% concentration. This study showed that the higher the extract concentration, the smaller the resulting NPs size compared to the lower concentration. It matched with earlier studies of AgNPs of *Spinacia oleracea* extract; 2% extract had a size of 173 nm, while 10% extract had a size of nm (Miranda et al., 2022). Although the sizes of AgNPs are also affected by other factors, the RSM result demonstrated that the extract concentration is not a significant factor.

pH is another crucial factor influencing the size, shape, and morphology of the synthesised AgNPs. The main influence of the reaction pH is its ability to alter the electrical charges of biomolecules, which can modify their reducing and capping abilities and the subsequent growth of NPs (Jain & Mehata, 2017). Figure 4d demonstrated the variation in the absorption spectrum of AgNPs synthesised at pH 4 and 10, with constant compositions of extract concentration 0.2% and temperature 50ºC, where pH 7 was not included in this variation as it adheres to the standard design of the BBD. At 0 hours, the detected SPR peak is only at pH 10, at 385 nm, indicating the formation of AgNPs. After 24 hours, a shift in SPR occurs at pH 10 to 406 nm, while at pH 4 experiences a decrease in intensity and no detected SPR peak. This significant difference is also supported by the colours, with pH 4 and pH 10 exhibiting light yellow to light purple (experiencing agglomeration) and yellowish to brownish-red, respectively. pH plays a role in regulating the redox reaction environment during the NPs formation. A lower pH results in a higher aggregation rate, leading to agglomeration (Fernando et al., 2020; Lau et al., 2016). A low pH creates an acidic condition where interparticle energy becomes neutral due to the presence of protons entering the neutrally charged AgNPs (Fernando & Zhou, 2019). On the other hand, pH 10 (higher pH) creates a base condition, leading to the stabilisation of hydroxyl ions and strengthening the negative charge (Wang et al., 2020). Similarly, in the earlier studies, pH 10 was identified as the optimal condition for the biosynthesis of AgNPs (Mardiyanto et al., 2023; Ndikau et al., 2017; Ndulini et al., 2024; Seifipour et al., 2020).

FT-IR Analysis

FT-IR spectroscopy analysis was conducted to identify the characteristic functional groups of *P. foetida* aqueous extract and PF-AgNPs that are related to the reduction and stabilisation of the NPs (Figure 5). The FT-IR spectrum of the *P. foetida* aqueous extract showed O-H stretching at 3256.48 cm^{-1}, indicating the presence of carbohydrates, proteins and polyphenols (Alkhulaifi et al., 2020; Bharadwaj et al., 2021; Kumari et al., 2020). The stretching vibrations of the C≡N (nitrite or nitrile) group were identified at 2118.59 cm^{-1}, and the C≡C (alkyne) around 2100 cm^{-1} (Jain & Mehata, 2017). The peak at 1593.13 cm^{-1} suggested the C=C stretching vibrations in double bonds for aromatic compounds or alkenes, as well as the vibrations of the carbonyl group C=O or amide (Arokiyaraj et

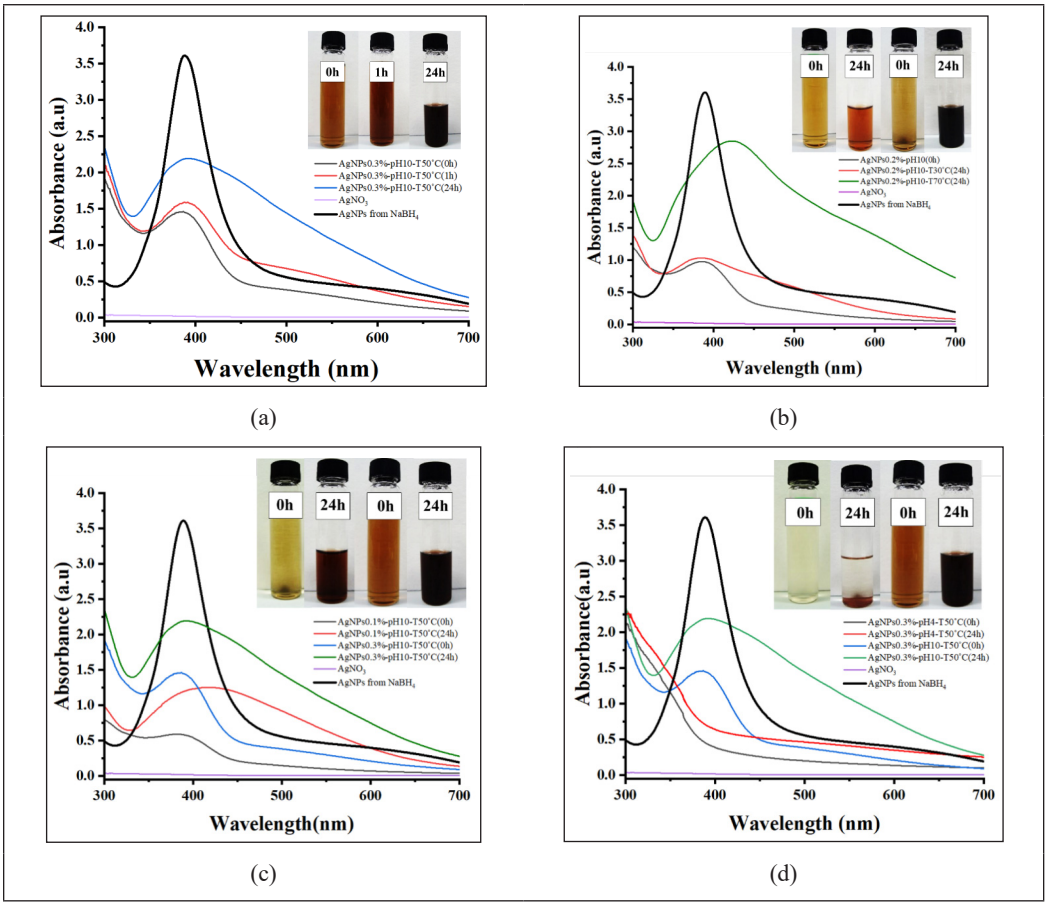

Figure 4. UV-visible spectroscopy results of the green synthesised PF-AgNPs: (a) effect of incubation time; (b) effect of temperature; (c) effect of extract concentration; and (d) effect of pH

al., 2014; Jaison et al., 2023). The bending (deformation) of C–H in aliphatic compounds was investigated by the presence of a band at 1399.44 cm^{-1} (Dobrucka, 2017). This band may also be associated with the symmetric vibration of the NO_2 group or the bending (deformation) of the C–H group in methyl ($-CH_3$) or methylene ($-CH_2^-$) groups (Mousavi et al., 2018). The stretching vibrations of the C-O bond of the alcohols and phenols at 1046.59 cm^{-1} (Riaz et al., 2022) or C-N, and 590.89 cm^{-1} indicates stretching vibrations of C-Cl (Nguyen et al., 2015).

Based on Figure 5a and Figure 5b, changes in the functional groups, as shown by the shift in absorption bands in comparison to the spectrum of *P. foetida* aqueous extracts as a standard, confirmed the successful formation of PF-AgNPs. Although the shifts were not highly pronounced, they were sufficient to suggest interactions between the active compounds in the extract and the synthesised PF-AgNPs. The vibrational data for the identified functional groups are summarised in Table 5. Remarkably, C-O-C stretching

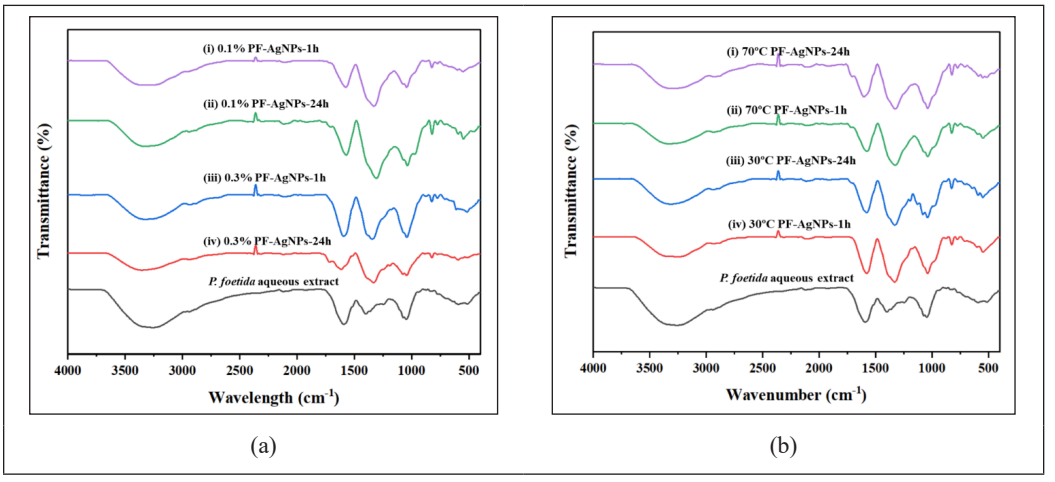

Figure 5. FTIR analysis of PF-AgNPs: (a) effect of concentration and (b) effect of temperature

Table 5
FT-IR peak assignments of P. foetida aqueous extract and synthesised PF-AgNPs

Possible assignments	*P. foetida* extract	PF-AgNPs (cm^{-1})			
		i	ii	iii	iv
Effect of different concentrations and reaction times (pH and temperature constant)					
v(O-H, H-bonding)	3256.48	3353.52	3326.07	3325.64	3352.54
v(C≡C or C≡N)	2118.59	ND	2115.72	ND	ND
v(C=C), Amide II	1593.13	1613.42	1592.9	1570.12	1574.11
v(C–H aliphatic)	1399.44	1331.61	1343.94	1307.72	1329.74
v(C–O)	1046.59	1043.08	1041.89	1036.77	1042.71
v(Aromatic C–H)	ND	823.57	824.1	822.85	823.48
v(Aromatic C–H), alkenes	ND	ND	775.32	ND	ND
v(C–Br or C–I)	590.89	594.36	517.12	547.62	552.47
Effect of different temperature and reaction times (pH and concentration constant)					
v(O-H, H-bonding)	3256.48	3280.98	3324.07	3238.57	3230.11
v(C≡C or C≡N)	2118.59	2114.89	2111.97	2116.14	2117.01
v(C=C), Amide II	1593.13	1603.29	1575.14	1577.99	1576.57
v(C–H aliphatic)	1399.44	1325.45	1326.8	1330.39	1330.27
v(C–O)	1046.59	1038.14	1038.44	1038.73	1039.13
v(Aromatic C–H)	ND	824.19	824.66	824.52	824.42
v(Aromatic C–H), alkenes	ND	773.51	774.18	775.1	775.13
v(C–Br or C–I)	590.89	550.01	548.55	547.27	547.36

Note. ND is not detected

identifies the fingerprint region of AgNPs spectra as identified at 1043, 1041, 1036, 1042, 1038, 1038, 1038, and 1039 cm^{-1} (Table 5). A larger shift in vibrational frequency frequently indicates a stronger interaction between the NPs and the capping agents. It is because the interaction can significantly alter the electronic environment around the functional groups involved, leading to more pronounced shifts in their vibrational frequencies (Jumabaev et al., 2025; Upadhyaya & Devi, 2018). Also, new peaks at 822.85-824.66 cm^{-1} and 773.51–753.2 cm^{-1} indicate C-H bending vibrations typical of aromatic compounds and alkenes, as well as suggest the presence of aromatic rings or unsaturated hydrocarbons (Khan et al., 2025). Additionally, the bands within the range of 517.12-594.36 cm^{-1} were identified as C-X stretching vibrations, as from halogenated compounds such as C-Cl or C-Br. These findings suggest that bioactive compounds such as flavonoids and alkaloids present in *P. foetida* extract play key roles in the reduction, formation, and stabilisation of the PF-AgNPs.

X-Ray Diffraction Analysis

The PF-AgNPs diffraction was compared with that of diffraction AgNPs prepared using $NaBH_4$ as a reducing agent as a standard reference for AgNPs formation. The XRD diffraction peaks of the $NaBH_4$-AgNPs appeared at 2θ angles of 38.08°, 44.25°, 64.37°, and 77.31°, whereas the PF-AgNPs incubated for 1 hour and 24 hours exhibited closely matching peaks at 2θ values of 38.08°, 44.26°, 64.39°, and 77.33°, and 38.07°, 44.24°, 64.36°, and 77.29°, respectively. These four peaks correspond to the (111), (200), (220), and (311) crystallographic planes of a face-centred cubic (fcc) structure, in accordance with the Joint Committee on Powder Diffraction Standards (JCPDS) file No. 04-0783.

These results confirm that the synthesised PF-AgNPs were crystalline and exhibited an fcc structure, which matched the values established earlier by (Anguraj et al., 2024; Elangovan et al., 2022; Khatun et al., 2024). The other peaks observed in Figure 6a were also identified as phytochemicals from the plant extract residue (Behravan et al., 2019; Elangovan et al., 2022; Jain & Mehata, 2017). Additionally, the diffractogram revealed a slight broadening in the (111) plane after about 24 hours of incubation as opposed to 1 hour, which suggested the beginning of NPs aggregation. Peak broadening may result from strain and defects in the crystal lattice caused by this aggregation process (Gulyaev et al., 2022).

SEM and EDX Analyses

The SEM analysis was conducted to investigate the synthesised PF-AgNPs' surface morphology, along with the EDX analysis to determine the elemental composition. The SEM image in Figure 6a showed that smaller NPs agglomerated, resulting in the formation of bigger-sized AgNPs agglomerates with a roughly spherical shape. This phenomenon was caused by an imbalance between attractive Van der Waals forces and repulsive electrostatic forces (Zhao et al., 2016). The short incubation time for PF-AgNPs did not provide

adequate time for phytochemicals to stabilise the NPs' surface effectively. Therefore, these agglomerations occurred (Giorgi et al., 2019). Such characteristics suggested that the formation of polydisperse AgNPs is due to variations in the phytochemical content of the *P. foetida* aqueous extract, which acts as both a reducing and stabilising agent.

According to Figure 6b, it was observed at 24-hour incubation and exhibited a more compact and uniform morphology, with relatively well-dispersed particles, although minor agglomeration was still observed. These results were consistent with the earlier established studies that AgNPs synthesised from *Crataegus pentagyna* at 1 µm magnification revealed improved stability and definition with longer incubation times (Ebrahimzadeh et al., 2020). The study concluded that extended incubation significantly enhances the formation of well-defined and stable AgNPs, owing to the increasingly effective stabilising action of phytochemicals over time. Further validated the presence of elemental silver, which confirmed the successful synthesis of PF-AgNPs using EDX analysis (Table 6),

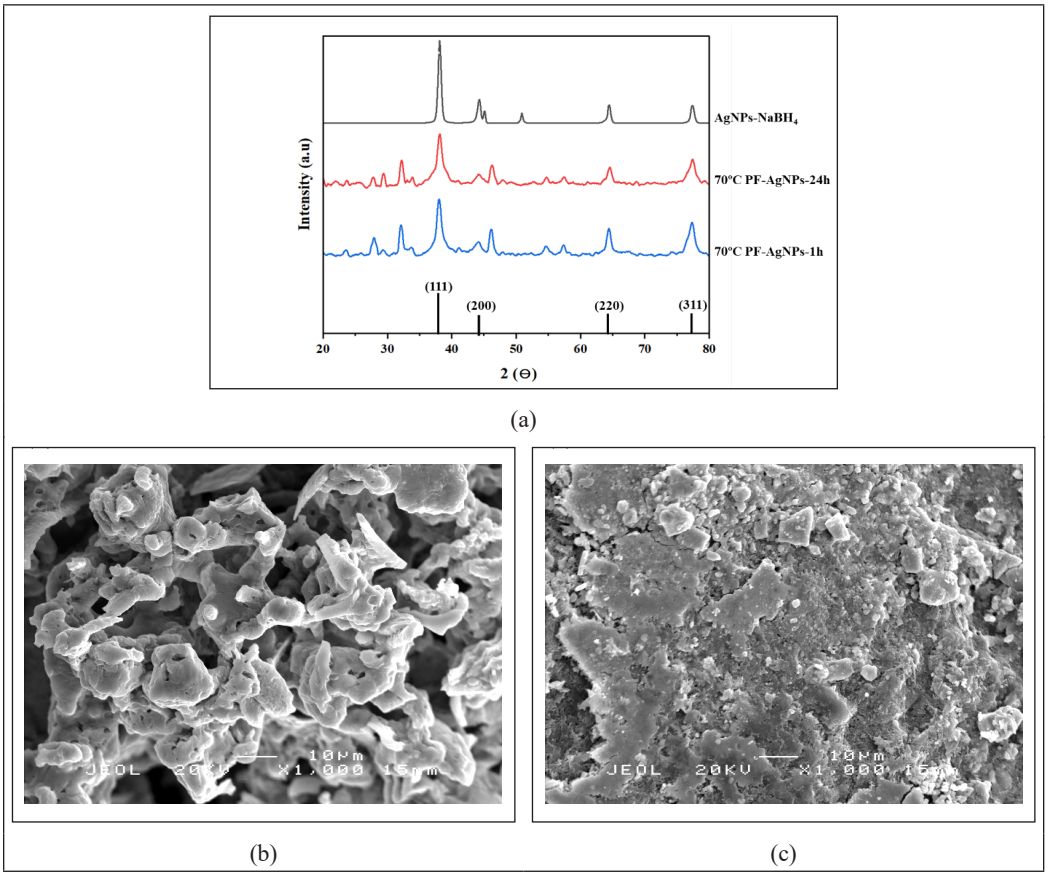

Figure 6. (a) XRD characterisation of PF-AgNPs; (b) SEM image after 1 h of incubation (10 µm scale, ×1000 magnification); (c) SEM image after 24 h of incubation (10 µm scale, ×1000 magnification) under optimal conditions

Table 6
Elemental composition using SEM-EDX at 1 and 24 h incubation time

Element	Mass (%) at 1 h	Mass (%) at 24 h	Atom (%)
Carbon (C)	18.33	8.75	28.40
Oxygen (O)	26.31	14.80	36.05
Sodium (Na)	4.91	1.61	2.72
Silicon (Si)	0.39	0.47	0.65
Chlorine (Cl)	2.89	4.41	4.84
Potassium (K)	1.60	0.85	0.85
Calcium (Ca)	0.53	2.13	2.07
Silver (Ag)	44.91	66.39	23.99

which revealed that, especially in this area, PF-AgNPs incubated for 24-hours contained a higher silver content (66.39%) compared to the 1-hour sample (44.91%). This result matched the result of the UV-Vis intensity, where 24-hour incubation has a higher intensity than 1-hour incubation time. Apart from this, the EDX analysis also detected elements such as Ca, K, Fe, and Si, potentially originating from residual plant extract components of *P. foetida*, which serve as capping and stabilising agents for the NPs' surfaces.

Proposed Mechanism of PF-AgNPs Synthesis

According to Ajitha et al. (2018), in the mechanism of the biosynthesised AgNPs formation, the Ag^{+} ions are reduced by antioxidant phytochemicals to Ag^{0} atoms, which then proceed through nucleation to create small clusters. The clusters then develop into petal-like structures and finally form flower-like superstructures with the assistance of bio-organic capping agents. The oxygen-containing functional groups (-OH and -COOH) participate in electrostatic attraction and complexation, enabling the particle to be stabilised. Phytochemicals not only function as reducing agents, but they also hinder further aggregation by capping the NPs through electron-rich hydroxyl groups. The study of Density of States (DOS) has also revealed that the interaction between Ag atoms and phenolic compounds is weakly adsorbed by the Van der Waals force or hydrogen bonds (Syafiuddin et al., 2017; Wang et al., 2021). This adsorption is reversible, does not change the basic structure of AgNPs and retains their stability and inherent properties such as electrical conductivity and catalytic behaviour (Brahmkhatri et al., 2015). The proposed reaction mechanism is summarised in Figure 7. This mechanism is supported by the UV-Vis spectra that displayed a characteristic SPR band at 420 nm and altered in colour from yellowish to brownish-red using optimum conditions. This reduction is pH-dependent to a certain extent, with basic conditions (pH 10) favouring the deprotonation of hydroxyl groups and enhancing reducing power capabilities. Further support is provided by the XRD patterns, which indicate that the NPs have an fcc crystalline structure, and FTIR spectra indicating the interaction of functional groups between the NPs and their capping agent.

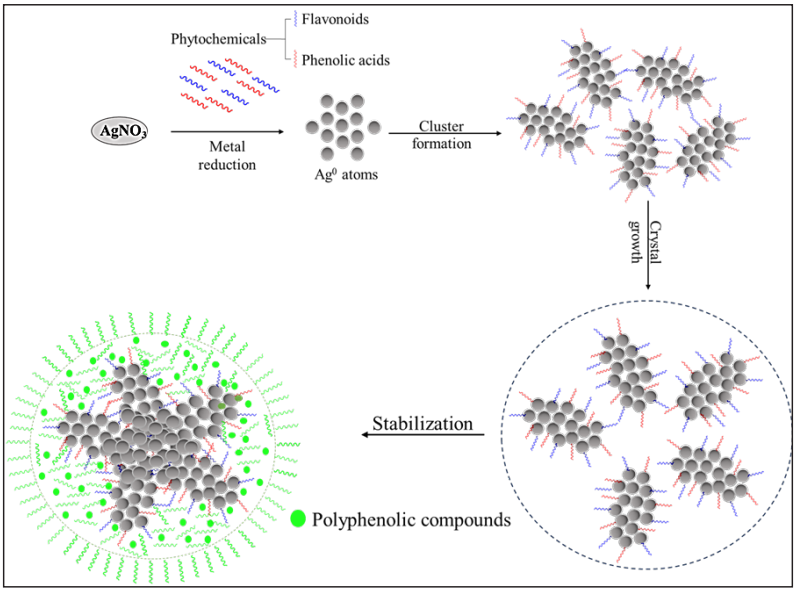

Figure 7. Mechanism of PF-AgNPs synthesis capped with *P. foetida* leaf extract, inspired by Ajitha et al. (2018)

Antioxidant Mechanism of PF-AgNPs

The antioxidant activity of PF-AgNPs is contributed by the combined actions of both the capping agents, such as phytochemicals, and the AgNPs (Figure 8a) (Javed et al., 2020). The antioxidative reactions of the stable purple DPPH radicals in an ideal model system result in their reduction to a pale, yellow-coloured DPPH–H through hydrogen atom transfer (HAT) and single electron transfer (SET) mechanisms, indicating DPPH radical scavenging capability. (Fouegue et al., 2018; Rohman et al., 2023; Wang et al., 2023). Polyphenolic groups in PF-AgNPs may donate hydrogen atoms or electrons to the DPPH radicals. These bioactive compounds are conjugated on the surface of AgNPs, especially those containing many hydroxyl groups, such as flavonoids. The AgNPs core also contributes to the reduction activity by: (1) increasing the amount of surface area available for interaction with free radicals; (2) facilitating electron transfer due to its metallic properties, and 3) stabilising phenoxy radicals generated by hydrogen donation, which prevents chain extension (Naseri et al., 2025; Park et al., 2016; Sytu & Camacho, 2018). In this assay, the control solution was dark purple, opposed to yellowish purple for PF-AgNPs with an inhibition of 35.64% (higher than that obtained in crude extract, i.e., 17.16%) under optimised conditions.

In NO radical scavenging assay, sodium nitroprusside (SNP) in aqueous solution at pH 7.4 undergoes spontaneous decomposition to generate NO• radicals that either interact with oxygen to produce nitrite ions (NO_2^-). Neutralisation of these reactive nitrogen species by PF-AgNPs occurs due to radical scavenging or metal chelation, as depicted in Figure 8b, adopted from Can et al. (2022) with a little modification. Antioxidant compounds

(ArOH) from phytochemical sources work as donors of hydrogen atoms or electrons for NO• radicals (Ermiş et al., 2025; Fraisse et al., 2018). In the hydrogen atom transfer mechanism, ArOH donates a hydrogen atom (H•) to neutralise the radical species, while ArOH itself is oxidised to a resonance-stabilised phenoxy radical. Furthermore, the antioxidants may operate through a SET mechanism to NO•, where an electron is donated to HNO, giving NO^- subsequently protonated to HNO. The formed ArO• radicals are stable, lack the initiation mechanism for a chain reaction and result in a decrease of free NO• radicals. This reduction in NO• level is witnessed with the decreased generation of nitrite in Griess reagent assay, and this indicates that PF-AgNPs have antioxidant scavenging ability (Can et al., 2022). In the experiment, PF-AgNPs exhibited the NO inhibitory activity at 38.70%.

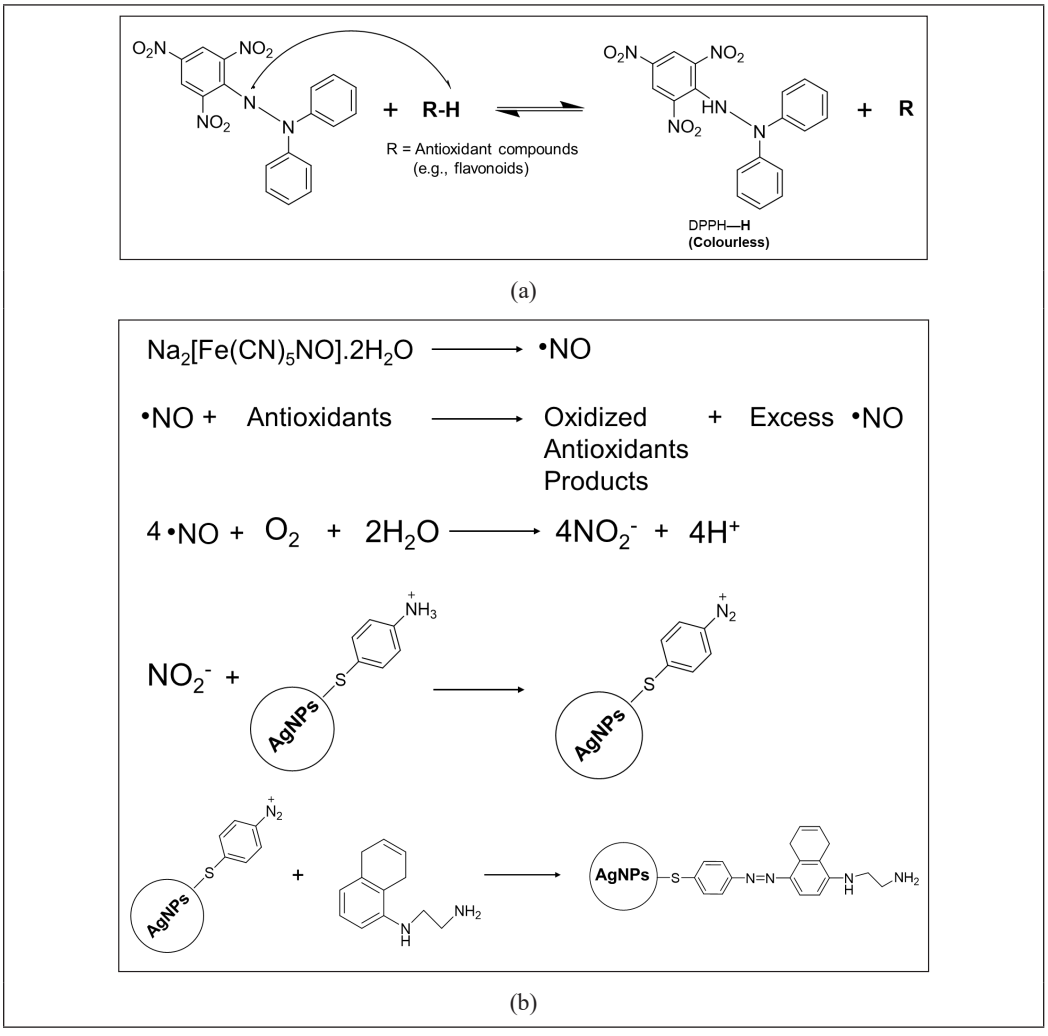

Figure 8. Proposed mechanisms of (a) DPPH; and (b) NO radical scavenging by antioxidants in PF-AgNPs

CONCLUSION

In this study, the green synthesis of PF-AgNPs was successfully optimised through Response Surface Methodology (RSM), identifying pH as the most influential factor in AgNPs formation. The optimal biosynthesis condition, 0.2% (w/v) extract at pH 10 and 70°C incubated for 24 hours, produced PF-AgNPs with significantly enhanced antioxidant activity compared to other formulations. The chemical profiling of the extract using ^{1}H NMR confirmed the presence of bioactive compounds, including flavonoid glycosides and other phytoconstituents, which are considered to play a role as natural reducing and stabilising agents during nanoparticle formation. Several other techniques, UV-Vis spectroscopy, FTIR, XRD, and SEM, have supported the synthesised nanoparticles to confirm that functional groups of phytochemical extracts helped the formation and stabilisation of nanoparticles and supported the synthesised nanoparticles' face-centred cubic (fcc) crystalline structure of silver, while SEM images revealed relatively uniform particles. Although polydispersity and lack of fit were observed in the NO-scavenger model, PF-AgNPs still exhibited enhanced antioxidant activity compared to the crude extract. Moreover, the therapeutic properties of PF-AgNPs could be evaluated for other biological activities, such as antimicrobial and anticancer effects. The integration of RSM with comprehensive physicochemical characterisation establishes a solid foundation for the development of eco-friendly AgNPs from natural resources. However, future studies, including in vivo evaluation and long-term stability assessment, should ideally incorporate particle size and zeta potential measurements using DLS to monitor nanoparticle homogeneity and colloidal stability, thereby supporting the sustainable production of low-cost PF-AgNPs with potential applications in biomedical, cosmetic, and environmental fields.

ACKNOWLEDGEMENT

We would like to thank the Ministry of Higher Education (MOHE) Malaysia for the financial support through the Fundamental Research Grant Scheme (FRGS/1/2022/STG02/UMT/02/1).

LIST OF ABBREVIATIONS

PF-AgNPs	:	*Passiflora foetida*-mediated silver nanoparticles
UV-Vis	:	Ultraviolet-visible spectroscopy
FTIR	:	Fourier transform infrared spectroscopy
XRD	:	X-ray diffraction
SEM	:	Scanning electron microscopy
EDX	:	Energy dispersive X-ray
SPR	:	Surface plasmon resonance

RSM	:	Response surface methodology
NO	:	Nitric oxide
DPPH	:	2,2-Diphenyl-1-picrylhydrazyl
^{1}H NMR	:	Proton nuclear magnetic resonance
ATR	:	Attenuated total reflectance
NP	:	Nanoparticle
RMSE	:	Root means square error
ANOVA	:	Analysis of variance
BBD	:	Box-Behnken design

REFERENCES

Abalkhil, T. A., Alharbi, S. A., Salmen, S. H., & Wainwright, M. (2017). Bactericidal activity of biosynthesised silver nanoparticles against human pathogenic bacteria. *Biotechnology & Biotechnological Equipment, 31*(2), 411-417. https://doi.org/10.1080/13102818.2016.1267594

Abdul-Hamid, N. A., Abas, F., Ismail, I. S., Tham, C. L., Maulidiani, M., Mediani, A., Swarup, S., & Umashankar, S. (2019). ^{1}H-NMR-based metabolomics to investigate the effects of *Phoenix dactylifera* seed extracts in LPS-IFN-γ-induced RAW 264.7 cells. *Food Research International, 125*, 108565.https://doi.org/10.1016/j.foodres.2019.108565

Abu-Elghait, M., Soliman, M. K. Y., Azab, M. S., & Salem, S. S. (2025). Response surface methodology: Optimisation of myco-synthesised gold and silver nanoparticles by *Trichoderma saturnisporum*. *Biomass Conversion and Biorefinery, 15*(3), 4211-4224. https://doi.org/10.1007/s13399-023-05188-4

Ajitha, B., Reddy, Y. A. K., Jeon, H. J., & Ahn, C. W. (2018). Synthesis of silver nanoparticles in an eco-friendly way using *Phyllanthus amarus* leaf extract: Antimicrobial and catalytic activity. *Advanced Powder Technology, 29*(1), 86-93. https://doi.org/10.1016/j.apt.2017.10.015

Akash, M. S. H., & Rehman, K. (2020). Ultraviolet-visible (UV-Vis) spectroscopy. In M. S. H. Akash & K. Rehman (Eds.), *Essentials of pharmaceutical analysis* (pp. 29-56). Springer Nature Singapore.https://doi.org/10.1007/978-981-15-1547-7_3

Alex, S. B., S., M. S., & L., M. S. (2025). Evaluation of antimicrobial, anti-inflammatory and cytotoxic effects of silver nanoparticles synthesised from *Cynodon dactylon*. *Natural Product Research, 39*(4), 779-786. https://doi.org/10.1080/14786419.2023.2290154

Al-Gebory, L., & Mengüç, M. P. (2018). The effect of pH on particle agglomeration and optical properties of nanoparticle suspensions. *Journal of Quantitative Spectroscopy and Radiative Transfer, 219*, 46-60. https://doi.org/10.1016/j.jqsrt.2018.07.020

Aliero, A. S., Zawawi, N. A., Malek, N. A. N. N., Usman, B. J., Asraf, M. H., Matmin, J., & Isah, M. (2024). Harnessing palm oil mill effluent for the green synthesis of silver nanoparticles: Optimisation via response surface methodology and assessment of antibacterial activity. *Journal of Inorganic and Organometallic Polymers and Materials*, 1-17. https://doi.org/10.1007/s10904-024-03478-6

Alkhulaifi, M. M., Alshehri, J. H., Alwehaibi, M. A., Awad, M. A., Al-Enazi, N. M., Aldosari, N. S., Hatamleh, A. A., & Abdel-Raouf, N. (2020). Green synthesis of silver nanoparticles using *Citrus limon* peels and

evaluation of their antibacterial and cytotoxic properties. *Saudi Journal of Biological Sciences, 27*(12), 3434-3441. https://doi.org/10.1016/j.sjbs.2020.09.031

Anguraj, A., Michael, H. S. R., Sugumaran, S., Madhusudhanan, G. R., & Sivaraman, R. K. (2024). A comparative study on biosynthesised silver nanoparticles from *Hylocereus undatus* fruit peel and their therapeutic applications. *Discover Nano, 19*(1), Article 49. https://doi.org/10.1186/s11671-024-03995-w

Arokiyaraj, S., Valan Arasu, M., Vincent, S., Oh, Y.-K., Kim, K. H., Choi, K.-C., Choi, S. H., & Prakash, N. U. (2014). Rapid green synthesis of silver nanoparticles from *Chrysanthemum indicum* L. and its antibacterial and cytotoxic effects: An in vitro study. *International Journal of Nanomedicine, 9*, 379-388. https://doi.org/10.2147/IJN.S53546

Barkat, M. A., Harshita, Beg, S., Naim, M. J., Pottoo, F. H., Singh, S. P., & Ahmad, F. J. (2017). Current progress in synthesis, characterisation and applications of silver nanoparticles: Precepts and prospects. *Recent Patents on Anti-Infective Drug Discovery, 13*(1), 53-69. https://doi.org/10.2174/1574891X12666171006102833

Behravan, M., Hossein Panahi, A., Naghizadeh, A., Ziaee, M., Mahdavi, R., & Mirzapour, A. (2019). Facile green synthesis of silver nanoparticles using *Berberis vulgaris* leaf and root aqueous extract and its antibacterial activity. *International Journal of Biological Macromolecules, 124*, 148-154.https://doi.org/10.1016/j.ijbiomac.2018.11.101

Bharadwaj, K. K., Rabha, B., Pati, S., Choudhury, B. K., Sarkar, T., Gogoi, S. K., Kakati, N., Baishya, D., Kari, Z. A., & Edinur, H. A. (2021). Green synthesis of silver nanoparticles using *Diospyros malabarica* fruit extract and assessment of their antimicrobial, anticancer and catalytic reduction of 4-nitrophenol (4-NP). *Nanomaterials, 11*(8), Article 1999.https://doi.org/10.3390/nano11081999

Brahmkhatri, V. P., Chandra, K., Dubey, A., & Atreya, H. S. (2015). An ultrastable conjugate of silver nanoparticles and protein formed through weak interactions. *Nanoscale, 7*(30), 12921-12931.https://doi.org/10.1039/C5NR03047A

Can, Z., Keskin, B., Üzer, A., & Apak, R. (2022). Detection of nitric oxide radical and determination of its scavenging activity by antioxidants using spectrophotometric and spectrofluorometric methods. *Talanta, 238*, 122993. https://doi.org/10.1016/j.talanta.2021.122993

Cativa, N. M., Dell'Erba, I. E., Waiman, C. V., Arenas, G. F., Ceolín, M., Giovanetti, L. J., Ramallo-López, J. M., Eliçabe, G., & Hoppe, C. E. (2020). Tuning the photothermal effect of carboxylated-coated silver nanoparticles through pH-induced reversible aggregation. *Langmuir, 36*(46), 13998-14008. https://doi.org/10.1021/acs.langmuir.0c02528

Corciovă, A., Mircea, C., Burlec, A. F., Fifere, A., Moleavin, I. T., Sarghi, A., Tuchiluş, C., Ivănescu, B., & Macovei, I. (2022). Green synthesis and characterisation of silver nanoparticles using a *Lythrum salicaria* extract and in vitro exploration of their biological activities. *Life, 12*(10), Article 1643.https://doi.org/10.3390/life12101643

Crisan, M. C., Teodora, M., & Lucian, M. (2021). Copper nanoparticles: Synthesis and characterisation, physiology, toxicity and antimicrobial applications. *Applied Sciences, 12*(1), Article 141. https://doi.org/10.3390/app12010141

De Silva, C., Nawawi, N. M., Abd Karim, M. M., Abd Gani, S., Masarudin, M. J., Gunasekaran, B., &

Ahmad, S. A. (2021). The mechanistic action of biosynthesised silver nanoparticles and its application in aquaculture and livestock industries. *Animals, 11*(7), Article 2097.https://doi.org/10.3390/ani11072097

Desai, K. M., Survase, S. A., Saudagar, P. S., Lele, S. S., & Singhal, R. S. (2008). Comparison of artificial neural network (ANN) and response surface methodology (RSM) in fermentation media optimisation: Case study of fermentative production of scleroglucan. *Biochemical Engineering Journal, 41*(3), 266-273. https://doi.org/10.1016/j.bej.2008.05.009

Díaz-Velasco, S., Delgado, J., Peña, F. J., & Estévez, M. (2022). Protein oxidation marker, α-amino adipic acid, impairs proteome of differentiated human enterocytes: Underlying toxicological mechanisms. *Biochimica et Biophysica Acta-Proteins and Proteomics, 1870*(7), Article 140797.https://doi.org/10.1016/j.bbapap.2022.140797

Dobrucka, R. (2017). Synthesis of titanium dioxide nanoparticles using *Echinacea purpurea* herba. *Iranian Journal of Pharmaceutical Research, 16*(2), 756-762. https://pmc.ncbi.nlm.nih.gov/articles/PMC5603885/

Ebrahimzadeh, Z., Salehzadeh, A., Naeemi, A. S., & Jalali, A. (2020). Silver nanoparticles biosynthesised by *Anabaena flos-aquae* enhance apoptosis in a breast cancer cell line. *Bulletin of Materials Science, 43*(1), Article 92. https://doi.org/10.1007/s12034-020-2064-1

Egodawaththa, N. M., Knight, A. L., Ma, J., Knight, D. A., Guisbert, E., & Nesnas, N. (2022). Synthesis and characterisation of ligand-stabilised silver nanoparticles and comparative antibacterial activity against *Escherichia coli*. *International Journal of Molecular Sciences, 23*(23), Article 15251.https://doi.org/10.3390/ijms232315251

Elangovan, D., Rahman, H. B. H., Dhandapani, R., Palanivel, V., Thangavelu, S., Paramasivam, R., & Muthupandian, S. (2022). Coating of wallpaper with green synthesised silver nanoparticles from *Passiflora foetida* fruit and its illustrated antifungal mechanism. *Process Biochemistry, 112*, 177-182. https://doi.org/10.1016/j.procbio.2021.11.027

Ermiş, S., Türk, Ş., Koç, Ö. K., Üzer, A., & Apak, R. (2025). Turn-on fluorometric assay based on functionalised gold nanoparticles for measurement of nitric oxide radical scavenging activity of phenol-, amine-, and thiol-type antioxidants. *Food Chemistry*, Article 146108. https://doi.org/10.1016/j.foodchem.2025.146108

Fernando, I., Tay, Y. Y., Karunasekera, H., & Zhou, Y. (2020). Observation of the interactions of silver nanoparticles (AgNPs) mediated by acid in aquatic matrices using in situ liquid cell transmission electron microscopy. *Analytica Chimica Acta, 1104*, 47-52. https://doi.org/10.1016/j.aca.2019.12.072

Fernando, I., & Zhou, Y. (2019). Impact of pH on the stability, dissolution and aggregation kinetics of silver nanoparticles. *Chemosphere, 216*, 297-305. https://doi.org/10.1016/j.chemosphere.2018.10.122

Fouegue, A. D. T., Mama, D. B., Ghogomu, J. N., Elie, Y., & Etoh, M.-A. (2018). The substitution effect on reaction enthalpies of antioxidant mechanisms of juglone and its derivatives in gas and solution phase: DFT study. *Journal of Chemistry, 2018*(1), Article 1958047. https://doi.org/10.1155/2018/1958047

Fraisse, D., Degerine-Roussel, A., Bred, A., Ndoye, S. F., Vivier, M., Felgines, C., & Senejoux, F. (2018). A novel HPLC method for direct detection of nitric oxide scavengers from complex plant matrices and its application to *Aloysia triphylla* leaves. *Molecules, 23*(7), Article 1574.https://doi.org/10.3390/molecules23071574

Gherasim, O., Puiu, R. A., Bîrca, A. C., Burduşel, A. C., & Grumezescu, A. M. (2020). An updated review

on silver nanoparticles in biomedicine. *Nanomaterials, 10*(11), Article 2318. https://doi.org/10.3390/nano10112318

Giorgi, F., Coglitore, D., Curran, J. M., Gilliland, D., Macko, P., Whelan, M., Worth, A., & Patterson, E. A. (2019). The influence of inter-particle forces on diffusion at the nanoscale. *Scientific Reports, 9*(1), Article 12325. https://doi.org/10.1038/s41598-019-48754-5

Gulyaev, V. P., Petrov, P. P., & Stepanova, K. V. (2022). Experimental validation of safety coefficient values of 09G2S steel by X-ray diffraction method. *Procedia Structural Integrity, 40*, 180-184.https://doi.org/10.1016/j.prostr.2022.04.024

Jain, S., & Mehata, M. S. (2017). Medicinal plant leaf extract and pure flavonoid mediated green synthesis of silver nanoparticles and their enhanced antibacterial property. *Scientific Reports, 7*(1), Article 15867. https://doi.org/10.1038/s41598-017-15724-8

Jaison, J. P., Balasubramanian, B., Gangwar, J., James, N., Pappuswamy, M., Anand, A. V., Al-Dhabi, N. A., Valan Arasu, M., Liu, W.-C., & Sebastian, J. K. (2023). Green synthesis of bioinspired nanoparticles mediated from plant extracts of Asteraceae family for potential biological applications. *Antibiotics, 12*(3), Article 543. https://doi.org/10.3390/antibiotics12030543

Javed, R., Zia, M., Naz, S., Aisida, S. O., Ain, N. ul, & Ao, Q. (2020). Role of capping agents in the application of nanoparticles in biomedicine and environmental remediation: Recent trends and future prospects. *Journal of Nanobiotechnology, 18*(1), Article 172. https://doi.org/10.1186/s12951-020-00704-4

Jumabaev, A., Khudaykulov, B., Holikulov, U., Norkulov, A., Subbiah, J., Al-Dossary, O. M., Hushvaktov, H., Absanov, A., & Issaoui, N. (2025). Molecular structure, vibrational spectral assignments, MEP, HOMO–LUMO, AIM, NCI, RDG, ELF and LOL properties of acetophenone and its solutions based on DFT calculations. *Optical Materials, 159*, Article 116683. https://doi.org/10.1016/j.optmat.2025.116683

Karan, T., Gonulalan, Z., Erenler, R., Kolemen, U., & Eminagaoglu, O. (2024). Green synthesis of silver nanoparticles using *Sambucus ebulus* leaves extract: Characterisation, quantitative analysis of bioactive molecules, antioxidant and antibacterial activities. *Journal of Molecular Structure, 1296*, Article 136836. https://doi.org/10.1016/j.molstruc.2023.136836

Kaushal, A., Khurana, I., Yadav, P., Allawadhi, P., Banothu, A. K., Neeradi, D., Thalugula, S., Barani, P. J., Naik, R. R., Navik, U., Bharani, K. K., & Khurana, A. (2023). Advances in therapeutic applications of silver nanoparticles. *Chemico-Biological Interactions, 382*, Article 110590.https://doi.org/10.1016/j.cbi.2023.110590

Khan, A., Younis, T., Anas, M., Ali, M., Shinwari, Z. K., Khalil, A. T., Munawar, K. S., Mohamed, H. E. A., Hkiri, K., & Maaza, M. (2025). *Withania coagulans*-mediated green synthesis of silver nanoparticles: Characterisation and assessment of their phytochemical, antioxidant, toxicity and antimicrobial activities. *BMC Plant Biology, 25*(1), Article 574. https://doi.org/10.1186/s12870-025-06533-7

Khanal, L. N., Dhakal, P. P., Kandel, M. R., Acharya, D., Baral, E. R., Chhetri, K., & Kalauni, S. K. (2023). Stem bark-mediated green synthesis of silver nanoparticles from *Pyrus pashia*: Characterisation, antioxidant and antibacterial properties. *Inorganics, 11*(6), Article 263. https://doi.org/10.3390/inorganics11060263

Khatun, H., Alam, S., Aziz, M. A., Karim, M. R., Rahman, M. H., Rabbi, M. A., & Habib, M. R. (2024).

Plant-assisted green preparation of silver nanoparticles using leaf extract of *Dalbergia sissoo* and their antioxidant, antibacterial and catalytic applications. *Bioprocess and Biosystems Engineering, 47*(8), 1347-1362. https://doi.org/10.1007/s00449-024-03029-w

Krishnamoorthi, R., Mahalingam, P. U., & Malaikozhundan, B. (2022). Edible mushroom extract engineered AgNPs as safe antimicrobial and antioxidant agents with no significant cytotoxicity on human dermal fibroblast cells. *Inorganic Chemistry Communications, 139*, Article 109362. https://doi.org/10.1016/j.inoche.2022.109362

Krupa, A. N. D., Abigail, M. E. A., Santhosh, C., Grace, A. N., & Vimala, R. (2016). Optimisation of process parameters for the microbial synthesis of silver nanoparticles using 3-level Box–Behnken design. *Ecological Engineering, 87*, 168-174. https://doi.org/10.1016/j.ecoleng.2015.11.030

Kumari, R., Saini, A. K., Kumar, A., & Saini, R. V. (2020). Apoptosis induction in lung and prostate cancer cells through silver nanoparticles synthesised from *Pinus roxburghii* bioactive fraction. *JBIC Journal of Biological Inorganic Chemistry, 25*(1), 23-37. https://doi.org/10.1007/s00775-019-01729-3

Lau, C. P., Abdul-Wahab, M. F., Jaafar, J., Chan, G. F., & Rashid, N. A. A. (2016). Effect of pH and biological media on polyvinylpyrrolidone-capped silver nanoparticles. *AIP Conference Proceedings, 1756*(1), Article 080002. https://doi.org/10.1063/1.4958781

Liu, H., Zhang, H., Wang, J., & Wei, J. (2020). Effect of temperature on the size of biosynthesised silver nanoparticles: Deep insight into microscopic kinetics analysis. *Arabian Journal of Chemistry, 13*(1), 1011-1019. https://doi.org/10.1016/j.arabjc.2017.09.004

Mardiyanto, M., Apriani, E. F., & Heylken, F. P. (2023). The role of temperature and pH in the synthesis of silver nanoparticles using *Areca catechu* L. seed extract as bioreductor. *Farmacia, 71*(2), 244-253.https://doi.org/10.31925/farmacia.2023.2.3

Maulidiani, M., Mediani, A., Abas, F., Park, Y. S., Park, Y.-K., Kim, Y. M., & Gorinstein, S. (2018). ^{1}H NMR and antioxidant profiles of polar and non-polar extracts of persimmon (*Diospyros kaki* L.): Metabolomics study based on cultivars and origins. *Talanta, 184*, 277-286. https://doi.org/10.1016/j.talanta.2018.02.084

Miranda, A., Akpobolokemi, T., Chung, E., Ren, G., & Raimi-Abraham, B. T. (2022). pH alteration in plant-mediated green synthesis and its resultant impact on antimicrobial properties of silver nanoparticles (AgNPs). *Antibiotics, 11*(11), Article 1592. https://doi.org/10.3390/antibiotics11111592

Mohamad Ali, B., Velavan, B., Sudhandiran, G., Sridevi, J., & Sultan Nasar, A. (2020). Radical dendrimers: Synthesis, anti-tumour activity and enhanced cytoprotective performance of TEMPO free radical functionalised polyurethane dendrimers. *European Polymer Journal, 122*, Article 109354.https://doi.org/10.1016/j.eurpolymj.2019.109354

Mouriya, G. K., Mohammed, M., Azmi, A. A., Khairul, W. M., Karunakaran, T., Amirul, A. A. A., Ramakrishna, S., Santhanam, R., & Vigneswari, S. (2023). Green synthesis of *Cicer arietinum* waste-derived silver nanoparticles for antimicrobial and cytotoxicity properties. *Biocatalysis and Agricultural Biotechnology, 47*, Article 102573. https://doi.org/10.1016/j.bcab.2022.102573

Mousavi, B., Tafvizi, F., & Zaker Bostanabad, S. (2018). Green synthesis of silver nanoparticles using *Artemisia turcomanica* leaf extract and the study of anti-cancer effect and apoptosis induction on gastric cancer cell line (AGS). *Artificial Cells, Nanomedicine, and Biotechnology, 46*(sup1), 499-510.https://doi.org/1

0.1080/21691401.2018.1430697

Naganthran, A., Verasoundarapandian, G., Khalid, F. E., Masarudin, M. J., Zulkharnain, A., Nawawi, N. M., Karim, M., Che Abdullah, C. A., & Ahmad, S. A. (2022). Synthesis, characterisation and biomedical application of silver nanoparticles. *Materials, 15*(2), Article 427.https://doi.org/10.3390/ma15020427

Naseri, M., Irannejad, M., Mehdilo, A., & Neisiani, R. K. (2025). Green synthesis of silver nanoparticles: A review of the methods and antioxidant properties of nanoparticles. *Amirkabir Journal of Civil Engineering, 57*(6), 939-972. https://doi.org/10.22060/ceej.2025.23714.8202

Ndikau, M., Noah, N. M., Andala, D. M., & Masika, E. (2017). Green synthesis and characterisation of silver nanoparticles using *Citrullus lanatus* fruit rind extract. *International Journal of Analytical Chemistry, 2017*, Article 8108504. https://doi.org/10.1155/2017/8108504

Ndulini, S. F., Mthembu, M. S., & Pullabhotla, V. S. R. (2024). *Ochrobactrum* bacterial-mediated pH-dependent synthesis of silver oxide nanoparticles. *BioNanoScience, 14*(3), 2092-2102. https://doi.org/10.1007/s12668-024-01470-5

Nguyen, T. Y., To, D. C., Tran, M. H., Lee, J. S., Lee, J. H., Kim, J. A., Woo, M. H., & Min, B. S. (2015). Anti-inflammatory flavonoids isolated from *Passiflora foetida*. *Natural Product Communications, 10*(6), Article 634. https://doi.org/10.1177/1934578X1501000634

Palanisamy, D. S., Gounder, B. S., Selvaraj, K., Kandhasamy, S., Alqahtani, T., Alqahtani, A., Chidambaram, K., Arunachalam, K., Alkahtani, A. M., Chandramoorthy, H. C., Sharma, N., Rajeshkumar, S., & Marwaha, L. (2024). Synergistic antibacterial and mosquitocidal effect of *Passiflora foetida*-synthesised silver nanoparticles. *Brazilian Journal of Biology, 84*, Article e263391. https://doi.org/10.1590/1519-6984.263391

Park, J., Cha, S.-H., Cho, S., & Park, Y. (2016). Green synthesis of gold and silver nanoparticles using gallic acid: Catalytic activity and conversion yield toward the 4-nitrophenol reduction reaction. *Journal of Nanoparticle Research, 18*(6), Article 166. https://doi.org/10.1007/s11051-016-3466-2

Patil, A., Lade, B., & Paikrao, H. (2015). A scientific update on *Passiflora foetida*. *European Journal of Medicinal Plants, 5*(2), 145-155.https://doi.org/10.9734/EJMP/2015/12015

Patil, N., Yadav, P., & Gogate, P. R. (2024). Ultrasound-assisted intensified enzymatic extraction of total phenolic compounds from pomegranate peels. *Separation and Purification Technology, 350*, Article 127967. https://doi.org/10.1016/j.seppur.2024.127967

Ponsuwan, K., Nathabumroong, S., Lekphrom, R., Sorin, S., Saengboonmee, C., Senawong, T., Tontapha, S., & Schevenels, F. T. (2024). Passifetilactones A–E, fatty acid lactones from the fruit and flowers of *Passiflora foetida* with cytotoxic activity. *Journal of Natural Products, 87*(6), 1652-1659.https://doi.org/10.1021/acs.jnatprod.4c00463

Pourmortazavi, S. M., Taghdiri, M., Makari, V., & Rahimi-Nasrabadi, M. (2015). Procedure optimisation for green synthesis of silver nanoparticles by aqueous extract of *Eucalyptus oleosa*. *Spectrochimica Acta Part A: Molecular and Biomolecular Spectroscopy, 136*, 1249-1254. https://doi.org/10.1016/j.saa.2014.10.010

Rajasekar, P., Palanisamy, S., Anjali, R., Vinosha, M., Thillaieswari, M., Malaikozhundan, B., Boomi, P., Saravanan, M., You, S. G., & Prabhu, N. M. (2019). *Cladophora fascicularis*-mediated silver nanoparticles: Assessment of their antibacterial activity against *Aeromonas hydrophila*. *Journal of Cluster Science,*

31(4), 673-683. https://doi.org/10.1007/s10876-019-01674-w

Riaz, M., Altaf, M., Ahmad, P., Khandaker, M. U., Osman, H., Eed, E. M., & Shakir, Y. (2022). Biogenic synthesis of Ag nanoparticles of 18.27 nm by *Zanthoxylum armatum* and determination of biological potentials. *Molecules, 27*(4), Article 1166. https://doi.org/10.3390/molecules27041166

Rohman, R., Nath, R., & Kar, R. (2023). Revisiting hydrogen atom transfer reactions through a simple and accurate theoretical model: Role of hydrogen bond energy in polyphenolic antioxidants. *Computational and Theoretical Chemistry, 1223*, Article 114097. https://doi.org/10.1016/j.comptc.2023.114097

Sati, A., Ranade, T. N., Mali, S. N., Ahmad Yasin, H. K., & Pratap, A. (2025). Silver nanoparticles (AgNPs): Comprehensive insights into bio/synthesis, key influencing factors, multifaceted applications and toxicity: A 2024 update. *ACS Omega, 10*(8), 7549-7582. https://doi.org/10.1021/acsomega.4c11045

Seifipour, R., Nozari, M., & Pishkar, L. (2020). Green synthesis of silver nanoparticles using *Tragopogon collinus* leaf extract and study of their antibacterial effects. *Journal of Inorganic and Organometallic Polymers and Materials, 30*(8), 2926-2936. https://doi.org/10.1007/s10904-020-01441-9

Shata, A. M., Rejili, M. S., El-Naggar, M. M., El-Asser, S. A., Saleh, A. A., Hafez, E. E., Haouala, F., & Youssef, A. S. (2025). Exploring the mechanisms and mode of action of bioactive compounds from marine *Streptomyces albidoflavus* against breast carcinoma cells. *BMC Biotechnology, 25*(1), Article 48.https://doi.org/10.1186/s12896-025-00991-5

Singh, J., Dutta, T., Kim, K.-H., Rawat, M., Samddar, P., & Kumar, P. (2018). Green synthesis of metals and their oxide nanoparticles: Applications for environmental remediation. *Journal of Nanobiotechnology, 16*(1), Article 84. https://doi.org/10.1186/s12951-018-0408-4

Song, Y., Wei, X.-Q., Li, M.-Y., Duan, X.-W., Sun, Y.-M., Yang, R.-L., Su, X.-D., Huang, R.-M., & Wang, H. (2018). Nutritional composition and antioxidant properties of the fruits of a Chinese wild *Passiflora foetida*. *Molecules, 23*(2), Article 459. https://doi.org/10.3390/molecules23020459

Sreejayan, & Rao, M. N. A. (1997). Nitric oxide scavenging by curcuminoids. *Journal of Pharmacy and Pharmacology, 49*(1), 105-107. https://doi.org/10.1111/j.2042-7158.1997.tb06761.x

Syafiuddin, A., Salmiati, Salim, M. R., Beng Hong Kueh, A., Hadibarata, T., & Nur, H. (2017). A review of silver nanoparticles: Research trends, global consumption, synthesis, properties and future challenges. *Journal of the Chinese Chemical Society, 64*(7), 732-756. https://doi.org/10.1002/jccs.201700067

Sytu, M. R. C., & Camacho, D. H. (2018). Green synthesis of silver nanoparticles (AgNPs) from *Lenzites betulina* and the potential synergistic effect of AgNPs and capping biomolecules in enhancing antioxidant activity. *BioNanoScience, 8*(3), 835-844. https://doi.org/10.1007/s12668-018-0548-x

Temur, N., Gundes, N. S., Korkmaz, B., Ozkaya, Z. A., & Ocsoy, I. (2024). Silver nanoparticles in dentistry. In *Silver nanoparticles for drug delivery* (pp. 265-288). Elsevier.https://doi.org/10.1016/B978-0-443-15343-3.00008-5

Upadhyaya, P., & Devi, T. G. (2018). Raman band shape analysis and DFT study of CO and CH stretching modes of N,N-dibutyl formamide in DMSO solvent. *Vibrational Spectroscopy, 96*, 110-117. https://doi.org/10.1016/j.vibspec.2018.03.006

Van Linh, N., Trung Tuong, N., Xuan Phong, P., Trang, D. T., Nhiem, N. X., Hoai An, D., & Huu Tai,

B. (2022). New phenylethanoid and other compounds from *Passiflora foetida* L., with their nitric oxide inhibitory activities. *Natural Product Communications, 17*(11), Article 141163. https://doi.org/10.1177/1934578X221141163

Wang, L., Periyasami, G., Aldalbahi, A., & Fogliano, V. (2021). The antimicrobial activity of silver nanoparticles biocomposite films depends on silver ion release behaviour. *Food Chemistry, 359*, Article 129859.https://doi.org/10.1016/j.foodchem.2021.129859

Wang, M., Mo, F., Li, H., Li, Y., Zhang, S., Zhu, L., Li, Z., Xu, J., Deng, N., & Wang, K. (2021). Adsorption based on weak interaction between phenolic hydroxyl and carboxyl groups and silver nanoparticles in aqueous environment: Experimental and DFT-D3 exploration. *Journal of Environmental Chemical Engineering, 9*(6), Article 106816. https://doi.org/10.1016/j.jece.2021.106816

Wang, X., Sun, T., Zhu, H., Han, T., Wang, J., & Dai, H. (2020). Roles of pH, cation valence and ionic strength in the stability and aggregation behaviour of zinc oxide nanoparticles. *Journal of Environmental Management, 267*, Article 110656. https://doi.org/10.1016/j.jenvman.2020.110656

Wang, Y., Liu, C., Tang, S., Tian, J., Wang, Y., & Yang, Y. (2023). Thermodynamics, kinetics and structure-activity relationship of hydroxyanthraquinones scavenging free radicals. *Food Bioscience, 53*, Article 102705. https://doi.org/10.1016/j.fbio.2023.102705

Wasilewska, A., Klekotka, U., Zambrzycka, M., Zambrowski, G., Święcicka, I., & Kalska-Szostko, B. (2023). Physico-chemical properties and antimicrobial activity of silver nanoparticles fabricated by green synthesis. *Food Chemistry, 400*, Article 133960. https://doi.org/10.1016/j.foodchem.2022.133960

Xu, M., Liu, G., Li, M., Huo, M., Zong, W., & Liu, R. (2020). Probing the cell apoptosis pathway induced by perfluorooctanoic acid and perfluorooctane sulfonate at the subcellular and molecular levels. *Journal of Agricultural and Food Chemistry, 68*(2), 633-641. https://doi.org/10.1021/acs.jafc.9b07072

Zhao, R., Luo, Y., & Pendry, J. B. (2016). Transformation optics applied to van der Waals interactions. *Science Bulletin, 61*(1), 59-67.https://doi.org/10.1007/s11434-015-0958-x

APPENDIX

1. Results of canonical path analysis for the intensity response

canonical.path(model2, dist = seq(-2, 2, by = 0.1))

	dist	x1	x2	x3	Temp	Conc	pH	yhat
1	-2.0	-3.211	0.567	-1.503	-14.22	0.2567	2.491	2.388
2	-1.9	-3.155	0.580	-1.422	-13.10	0.2580	2.734	2.208
3	-1.8	-3.098	0.593	-1.340	-11.96	0.2593	2.980	2.035
4	-1.7	-3.041	0.606	-1.259	-10.82	0.2606	3.223	1.873
5	-1.6	-2.985	0.619	-1.177	-9.70	0.2619	3.469	1.719
6	-1.5	-2.928	0.631	-1.096	-8.56	0.2631	3.712	1.575
7	-1.4	-2.871	0.644	-1.015	-7.42	0.2644	3.955	1.441
8	-1.3	-2.815	0.657	-0.933	-6.30	0.2657	4.201	1.315
9	-1.2	-2.758	0.670	-0.852	-5.16	0.2670	4.444	1.199
10	-1.1	-2.702	0.683	-0.770	-4.04	0.2683	4.690	1.092
11	-1.0	-2.645	0.695	-0.689	-2.90	0.2695	4.933	0.995
12	-0.9	-2.588	0.708	-0.608	-1.76	0.2708	5.176	0.906
13	-0.8	-2.532	0.721	-0.526	-0.64	0.2721	5.422	0.827
14	-0.7	-2.475	0.734	-0.445	0.50	0.2734	5.665	0.758
15	-0.6	-2.418	0.747	-0.363	1.64	0.2747	5.911	0.697
16	-0.5	-2.362	0.760	-0.282	2.76	0.2760	6.154	0.646
17	-0.4	-2.305	0.772	-0.201	3.90	0.2772	6.397	0.604
18	-0.3	-2.248	0.785	-0.119	5.04	0.2785	6.643	0.572
19	-0.2	-2.192	0.798	-0.038	6.16	0.2798	6.886	0.549
20	-0.1	-2.135	0.811	0.044	7.30	0.2811	7.132	0.534
21	0.0	-2.079	0.824	0.125	8.42	0.2824	7.375	0.530
22	0.1	-2.022	0.836	0.207	9.56	0.2836	7.621	0.535
23	0.2	-1.965	0.849	0.288	10.70	0.2849	7.864	0.548
24	0.3	-1.909	0.862	0.369	11.82	0.2862	8.107	0.572
25	0.4	-1.852	0.875	0.451	12.96	0.2875	8.353	0.604
26	0.5	-1.795	0.888	0.532	14.10	0.2888	8.596	0.646
27	0.6	-1.739	0.900	0.614	15.22	0.2900	8.842	0.697
28	0.7	-1.682	0.913	0.695	16.36	0.2913	9.085	0.758
29	0.8	-1.625	0.926	0.776	17.50	0.2926	9.328	0.827
30	0.9	-1.569	0.939	0.858	18.62	0.2939	9.574	0.906
31	1.0	-1.512	0.952	0.939	19.76	0.2952	9.817	0.995
32	1.1	-1.455	0.964	1.021	20.90	0.2964	10.063	1.093
33	1.2	-1.399	0.977	1.102	22.02	0.2977	10.306	1.199
34	1.3	-1.342	0.990	1.183	23.16	0.2990	10.549	1.315
35	1.4	-1.286	1.003	1.265	24.28	0.3003	10.795	1.441
36	1.5	-1.229	1.016	1.346	25.42	0.3016	11.038	1.575
37	1.6	-1.172	1.029	1.428	26.56	0.3029	11.284	1.720
38	1.7	-1.116	1.041	1.509	27.68	0.3041	11.527	1.872
39	1.8	-1.059	1.054	1.591	28.82	0.3054	11.773	2.036
40	1.9	-1.002	1.067	1.672	29.96	0.3067	12.016	2.208
41	2.0	-0.946	1.080	1.753	31.08	0.3080	12.259	2.388

2. Results of canonical path analysis for the NO response

canonical.path(model2, dist = seq(-2, 2, by = 0.1))

	dist	x1	x2	x3	Temp	Conc	pH	yhat
1	-2.0	-1.129	1.827	-1.390	27.42	0.3827	2.830	40.454
2	-1.9	-1.105	1.775	-1.308	27.90	0.3775	3.076	38.733
3	-1.8	-1.082	1.724	-1.225	28.36	0.3724	3.325	37.099
4	-1.7	-1.058	1.672	-1.143	28.84	0.3672	3.571	35.555
5	-1.6	-1.034	1.621	-1.060	29.32	0.3621	3.820	34.094
6	-1.5	-1.011	1.569	-0.978	29.78	0.3569	4.066	32.730
7	-1.4	-0.987	1.518	-0.896	30.26	0.3518	4.312	31.457
8	-1.3	-0.963	1.467	-0.813	30.74	0.3467	4.561	30.262
9	-1.2	-0.940	1.415	-0.731	31.20	0.3415	4.807	29.161
10	-1.1	-0.916	1.364	-0.648	31.68	0.3364	5.056	28.143
11	-1.0	-0.892	1.312	-0.566	32.16	0.3312	5.302	27.216
12	-0.9	-0.869	1.261	-0.483	32.62	0.3261	5.551	26.378
13	-0.8	-0.845	1.209	-0.401	33.10	0.3209	5.797	25.628
14	-0.7	-0.821	1.158	-0.319	33.58	0.3158	6.043	24.969
15	-0.6	-0.797	1.107	-0.236	34.06	0.3107	6.292	24.394
16	-0.5	-0.774	1.055	-0.154	34.52	0.3055	6.538	23.910
17	-0.4	-0.750	1.004	-0.071	35.00	0.3004	6.787	23.511
18	-0.3	-0.726	0.952	0.011	35.48	0.2952	7.033	23.202
19	-0.2	-0.703	0.901	0.094	35.94	0.2901	7.282	22.982
20	-0.1	-0.679	0.850	0.176	36.42	0.2850	7.528	22.850
21	0.0	-0.655	0.798	0.258	36.90	0.2798	7.774	22.806
22	0.1	-0.632	0.747	0.341	37.36	0.2747	8.023	22.850
23	0.2	-0.608	0.695	0.423	37.84	0.2695	8.269	22.982
24	0.3	-0.584	0.644	0.506	38.32	0.2644	8.518	23.204
25	0.4	-0.561	0.592	0.588	38.78	0.2592	8.764	23.512
26	0.5	-0.537	0.541	0.671	39.26	0.2541	9.013	23.910
27	0.6	-0.513	0.490	0.753	39.74	0.2490	9.259	24.393
28	0.7	-0.490	0.438	0.835	40.20	0.2438	9.505	24.965
29	0.8	-0.466	0.387	0.918	40.68	0.2387	9.754	25.629
30	0.9	-0.442	0.335	1.000	41.16	0.2335	10.000	26.379
31	1.0	-0.418	0.284	1.083	41.64	0.2284	10.249	27.220
32	1.1	-0.395	0.232	1.165	42.10	0.2232	10.495	28.145
33	1.2	-0.371	0.181	1.248	42.58	0.2181	10.744	29.163
34	1.3	-0.347	0.130	1.330	43.06	0.2130	10.990	30.261
35	1.4	-0.324	0.078	1.412	43.52	0.2078	11.236	31.449
36	1.5	-0.300	0.027	1.495	44.00	0.2027	11.485	32.733
37	1.6	-0.276	-0.025	1.577	44.48	0.1975	11.731	34.101
38	1.7	-0.253	-0.076	1.660	44.94	0.1924	11.980	35.558
39	1.8	-0.229	-0.127	1.742	45.42	0.1873	12.226	37.094
40	1.9	-0.205	-0.179	1.825	45.90	0.1821	12.475	38.740
41	2.0	-0.182	-0.230	1.907	46.36	0.1770	12.721	40.448

3. Results of canonical path analysis for the DPPH response

> canonical.path(model2, dist = seq(-2, 2, by = 0.1))

	dist	x1	x2	x3	Temp	Conc	pH	yhat
1	-2.0	-2.190	-0.384	0.218	6.20	0.1616	7.654	52.327
2	-1.9	-2.094	-0.370	0.244	8.12	0.1630	7.732	48.713
3	-1.8	-1.999	-0.357	0.271	10.02	0.1643	7.813	45.313
4	-1.7	-1.903	-0.343	0.297	11.94	0.1657	7.891	42.071
5	-1.6	-1.808	-0.329	0.323	13.84	0.1671	7.969	39.042
6	-1.5	-1.712	-0.316	0.350	15.76	0.1684	8.050	36.167
7	-1.4	-1.617	-0.302	0.376	17.66	0.1698	8.128	33.505
8	-1.3	-1.521	-0.288	0.403	19.58	0.1712	8.209	30.998
9	-1.2	-1.426	-0.275	0.429	21.48	0.1725	8.287	28.707
10	-1.1	-1.330	-0.261	0.455	23.40	0.1739	8.365	26.576
11	-1.0	-1.235	-0.247	0.482	25.30	0.1753	8.446	24.644
12	-0.9	-1.139	-0.233	0.508	27.22	0.1767	8.524	22.884
13	-0.8	-1.044	-0.220	0.534	29.12	0.1780	8.602	21.327
14	-0.7	-0.949	-0.206	0.561	31.02	0.1794	8.683	19.946
15	-0.6	-0.853	-0.192	0.587	32.94	0.1808	8.761	18.741
16	-0.5	-0.758	-0.179	0.613	34.84	0.1821	8.839	17.733
17	-0.4	-0.662	-0.165	0.640	36.76	0.1835	8.920	16.896
18	-0.3	-0.567	-0.151	0.666	38.66	0.1849	8.998	16.253
19	-0.2	-0.471	-0.137	0.692	40.58	0.1863	9.076	15.790
20	-0.1	-0.376	-0.124	0.719	42.48	0.1876	9.157	15.514
21	0.0	-0.280	-0.110	0.745	44.40	0.1890	9.235	15.421
22	0.1	-0.185	-0.096	0.771	46.30	0.1904	9.313	15.513
23	0.2	-0.089	-0.083	0.798	48.22	0.1917	9.394	15.791
24	0.3	0.006	-0.069	0.824	50.12	0.1931	9.472	16.249
25	0.4	0.102	-0.055	0.851	52.04	0.1945	9.553	16.899
26	0.5	0.197	-0.042	0.877	53.94	0.1958	9.631	17.724
27	0.6	0.293	-0.028	0.903	55.86	0.1972	9.709	18.743
28	0.7	0.388	-0.014	0.930	57.76	0.1986	9.790	19.940
29	0.8	0.484	0.000	0.956	59.68	0.2000	9.868	21.330
30	0.9	0.579	0.013	0.982	61.58	0.2013	9.946	22.887
31	1.0	0.675	0.027	1.009	63.50	0.2027	10.027	24.653
32	1.1	0.770	0.041	1.035	65.40	0.2041	10.105	26.580
33	1.2	0.866	0.054	1.061	67.32	0.2054	10.183	28.708
34	1.3	0.961	0.068	1.088	69.22	0.2068	10.264	31.009
35	1.4	1.057	0.082	1.114	71.14	0.2082	10.342	33.510
36	1.5	1.152	0.096	1.140	73.04	0.2096	10.420	36.172
37	1.6	1.248	0.109	1.167	74.96	0.2109	10.501	39.048
38	1.7	1.343	0.123	1.193	76.86	0.2123	10.579	42.077
39	1.8	1.439	0.137	1.219	78.78	0.2137	10.657	45.320
40	1.9	1.534	0.150	1.246	80.68	0.2150	10.738	48.720
41	2.0	1.630	0.164	1.272	82.60	0.2164	10.816	52.334